

Neuregulin 1 and ErbB4 Kinase Actively Regulate Sharp Wave Ripples in the Hippocampus

Heath L. Robinson,¹ Zhibing Tan,¹ Ivan Santiago-Marrero,¹ Emily P. Arzola,¹ Timothy Vladimir Dong,¹ Wen-Cheng Xiong,^{1,2} and Lin Mei^{1,2}

¹Department of Neurosciences, School of Medicine, Case Western Reserve University, Cleveland, Ohio 44106, and ²Louis Stokes Cleveland Veterans Affairs Medical Center, Cleveland, Ohio 44106

Sharp wave ripples (SW-Rs) in the hippocampus are synchronized bursts of hippocampal pyramidal neurons (PyNs), critical for spatial working memory. However, the molecular underpinnings of SW-Rs remain poorly understood. We show that SW-Rs in hippocampal slices from both male and female mice were suppressed by neuregulin 1 (NRG1), an epidermal growth factor whose expression is enhanced by neuronal activity. Pharmacological inhibition of ErbB4, a receptor tyrosine kinase for NRG1, increases SW-R occurrence rate in hippocampal slices. These results suggest an important role of NRG1-ErbB4 signaling in regulating SW-Rs. To further test this notion, we characterized SW-Rs in freely moving male mice, chemical genetic mutant mice, where ErbB4 can be specifically inhibited by the bulky inhibitor 1NMPP1. Remarkably, SW-R occurrence was increased by 1NMPP1. We found that 1NMPP1 increased the firing rate of PyN neurons, yet disrupted PyN neuron dynamics during SW-R events. Furthermore, 1NMPP1 increased SW-R occurrence during both nonrapid eye movement (NREM) sleep states and wake states with a greater impact on SW-Rs during wake states. In accord, spatial working memory was attenuated in male mice. Together these results indicate that dynamic activity of ErbB4 kinase is critical to SW-Rs and spatial working memory. This study reveals a novel regulatory mechanism of SW-Rs and a novel function of the NRG1-ErbB4 signaling.

Key words: hippocampus; molecular-cellular; neuregulin-ErbB4; sharp wave ripples; spatial working memory; synaptic

Significance Statement

Sharp wave ripples (SW-Rs) are a hippocampal event, important for memory functioning. Yet the molecular pathways that regulate SW-Rs remain unclear. Neuregulin 1 (NRG1), previously known to be increased in pyramidal neuron's (PyNs) in an activity dependent manner, signals to its receptor, ErbB4 kinase, that is an important regulator of GABAergic transmission and long-term potentiation in the hippocampus. Our findings demonstrate that SW-Rs are regulated by this signaling pathway in a dynamic manner. Not only so, we show that this signaling pathway is dynamically needed for spatial working memory. These data suggest a molecular signaling pathway, NRG1-ErbB4, that regulates an important network event of the hippocampus, SW-Rs, that underlies memory functioning.

Introduction

The hippocampus is critical to learning and memory. Hippocampal activity increases and correlates with spatial related memories and decreases in patients with temporal lobe damage (Abrahams et al., 1997; Maguire et al., 1998). In rodents, lesioning the hippocampus impairs memory (Kim and Frank, 2009;

Broadbent et al., 2010). The hippocampus produces rhythmical slow activity during movement and large irregular activity during immobility (Whishaw and Vanderwolf, 1971; Kay and Frank, 2019), which consist of activity bursts with negative sharp waves, termed sharp wave ripples (SW-Rs; Buzsáki et al., 1983). Neurons whose field assemblies reflect trajectories through space are reactivated in a time-compressed cascade during SW-Rs (O'Neill et al., 2006; Diba and Buzsáki, 2007). Impairing SW-Rs disrupts, while increasing SW-R length, improves spatial working memory (Girardeau et al., 2009; Ego-Stengel and Wilson, 2010; Jadhav et al., 2012; Fernández-Ruiz et al., 2019). SW-R replay is fundamental to memory consolidation during nonrapid eye movement (NREM) states of sleep and to retrieval and updating of navigational planning during wake states (Wilson and McNaughton, 1994; Buzsáki, 2015; Joo and Frank, 2018). Interneurons (INs) are critical to the manifestation of SW-Rs (Klausberger and Somogyi, 2008). SW-Rs are associated with

Received May 15, 2021; revised Oct. 19, 2021; accepted Nov. 20, 2021.

Author contributions: H.L.R., Z.T., W.-C.X., and L.M. designed research; H.L.R., Z.T., I.S.-M., E.P.A., and T.V.D. performed research; L.M. contributed unpublished reagents/analytic tools; H.L.R. analyzed data; H.L.R. wrote the first draft of the paper; H.L.R. and L.M. edited the paper; H.L.R. and L.M. wrote the paper.

This work was supported by the National Institutes of Health Grant MH083317 (to L.M.). We thank Dr. Azahara Oliva and Dr. Antonio Fernández-Ruiz for helpful comments on the manuscript, as well as members of the L.M. and W.-C.X. labs for discussion.

The authors declare no competing financial interests.

Correspondence should be addressed to Lin Mei at lin.mei@case.edu.

<https://doi.org/10.1523/JNEUROSCI.1022-21.2021>

Copyright © 2022 the authors

increased IN firing (Csicsvari et al., 1999; Klausberger et al., 2004) and potentiated by inhibition of GABAA receptors (Maier et al., 2003; Papatheodoropoulos et al., 2007). Optogenetic stimulation and inhibition induce and disrupt SW-Rs, respectively (Schlingloff et al., 2014; Gan et al., 2017). However, molecular mechanisms that regulate SW-Rs remain poorly understood.

Neuregulin 1 (NRG1) is a growth factor that activates the receptor tyrosine kinase ErbB4 (Mei and Xiong, 2008; Mei and Nave, 2014). NRG1 is produced mainly in PyNs in an activity-dependent manner (Eilam et al., 1998; Ozaki et al., 2004; Liu et al., 2011; Tan et al., 2012). ErbB4 is expressed specifically in GABAergic INs in the hippocampus (Vullhorst et al., 2009; Fazzari et al., 2010; Bean et al., 2014). NRG1, via ErbB4, increases GABA release, suppresses the firing of PyNs and inhibits LTP (Huang et al., 2000; Woo et al., 2007; Pitcher et al., 2008; Chen et al., 2010; Tan et al., 2018). Deletion of ErbB4 in INs increased γ oscillations (Del Pino et al., 2013; Tan et al., 2018), while NRG1 increases carbachol-induced γ oscillations in hippocampal slices (Fisahn et al., 2009). Spatial working memory and contextual fear conditioning are impaired in mutant mice where ErbB4 is deleted in INs (Wen et al., 2010; Del Pino et al., 2013, 2017; Wang et al., 2018) or specifically inhibited in a chemical genetic ErbB4 mutant mouse (Tan et al., 2018). These data highlight an important role of ErbB4 kinase activity in hippocampus-related behaviors.

Considering that GABA release is maintained by the NRG1-ErbB4 signaling in the hippocampus, we investigated whether it regulates SW-Rs. We studied the effects of exogenous NRG1 and ErbB4 inhibition on SW-Rs in hippocampal slices and explored ErbB4 kinase's impact *in vivo* on SW-Rs by recording freely moving mice. We found that NRG1 reduces and ErbB4 inhibition increases SW-R occurrence in hippocampal slices and *in vivo*. By analyzing neuronal firing, we found that acute inhibition of ErbB4 increases the firing rate of hippocampal PyNs and disrupts PyN dynamics of SW-R events. Furthermore, ErbB4 inhibition increased SW-R events more in wake states than in NREM states. Concomitantly, ErbB4 inhibition attenuates spatial working memory. These results reveal a novel regulatory mechanism of SW-Rs by the NRG1-ErbB4 signaling.

Materials and Methods

Animals

Male and female mice were maintained on a 12/12 h light/dark cycle with *ad libitum* access to food and water. T796G mice were described previously (Tan et al., 2018). Wild-type C57BL/6J mice were used (The Jackson Laboratory, stock #000664). For genotyping, wild-type allele primers were as follows: forward, 5'-GATCT GCAGA TCAAT TCAC-3', reverse, 5'-GCCAA CCAAC TGGAT AGTG-3'; T796G allele primers were as follows: forward, 5'-AACTG AATTC ACTTT GTGG-3', reverse, 5'-CTGTA GCAGC AACAA TAGC-3'. Mice were maintained as described previously (Tan et al., 2018). All experiments conformed to the guidelines of the National Institutes of Health were approved by the Institutional Animal Care and Use Committee (IACUC) of Case Western Reserve University.

Behavioral analysis

For behavioral experiments, 8- to 12-week male mice were used. The W-maze was designed using an open-source 3D software (FreeCAD) that is available on request or found online (https://github.com/heathlarsson/w_maze_3d_design) and printed by Digilab 3D45 (Dremel). Dimensions of the maze were 76 cm by 64 cm with arms 12 cm wide and 66 cm long. The inside arm was printed black and outside arms printed white, to distinguish inside versus outside (Frank et al., 2000). Mice were food-deprived to 85% of the body weight with *ad libitum* access to food, as described previously (Tan et al., 2018). Mice were switched from normal chow to food pellets

(LabTab 5TUL Purified Rodent Tablets, Test Diet) and maintained at target weight throughout training and experiments. After one week on food pellet diet with stable maintenance of 85% body weight, mice were habituated to one arm of the W-maze with reward chambers on either side. Pellets were spread throughout the arm for the first 2 d, and switched to reward chambers for two more days. Next, animals were administered pellets at the end of each arm until animals easily retrieved pellets at each end (~1–4 d). After training on a single arm, animals were trained to retrieve pellets on two arms, switching outbound arms each day. After animals retrieved pellets on both sets of two arms (~3–6 d), animals were trained on the three arms until able to perform at >85% accuracy on both inbound and outbound arms (~10–14 d). An animal was only given pellet when full body had passed the entrance of an arm. All sessions were videotaped, including experimenter. Video data were postprocessed using ANY-maze software (Stoelting Co) for behavioral analysis.

Slice recording

For slices recording, 4- to 12-week-old male and female mice were used. Mice were anesthetized with isoflurane and subjected to cardiac perfusion with ice-cold highly oxygenated (95% O₂ and 5% CO₂) artificial CSF (ACSF) before decapitation. Brains were rapidly removed and placed in ice-cold oxygenated ACSF. ACSF contains the following: 125 mM NaCl, 2.5 mM KCl, 2 mM CaCl₂, 1.3 mM MgCl₂, 1.3 mM NaH₂PO₄, 25 mM NaHCO₃, and 10 mM glucose. Horizontal slices (~450 μ m) were cut on agarose gel at an angle (~12°) using a vibratome (VT1200, Leica) and incubated in oxygenated ACSF at 34°C for 1.5 h before recording (Norimoto et al., 2012).

Slices were transferred from incubation chamber to dual superfusion chamber that exposed both sides of horizontal slices to flowing, oxygenated ACSF at 34°C. ACSF flowed continuously and directly onto slices at 6 ml/min (Maier et al., 2003; Norimoto et al., 2012, 2018). Slices were visualized using infrared video microscopy and differential interference contrast optics under a microscope (BX51W1, Olympus). Recording electrodes were made from borosilicate glass capillaries (B-120-69-15, Sutter Instruments) with resistance in the range 0.5–1 M Ω filled with ACSF. They were inserted into the superficial portion of the pyramidal layer of the CA1, where positive deflections of SW-Rs were largest (Maier et al., 2003; Norimoto et al., 2012). Field potentials (FPs) were recorded with an Axon 700B patch clamp amplifier and Axon Digidata 1550B sampled at 10 kHz (Molecular Devices LLC). Signals were band-pass filtered to 0.5–1000 Hz using Clampex 9.0 (Molecular Devices LLC). Slices were allowed at least 10 min of acclimation once transferred to recording chamber and SW-R events were readily observable after recording electrodes were positioned.

Tetrode construction and implantation

For *in vivo* recording, 8- to 12-week male animals were used. Electrodes (eight) were made by first constructing tetrodes folded, twisted, and fastened together with low heat (Lin et al., 2006; Fox et al., 2017; Tan et al., 2018; 10% iridium, 90% platinum, California Fine Wire Company). Tetrodes (eight tetrodes) were inserted into polyimide tubing (inner diameter 200.5 μ m; outer diameter 254.1 μ m, Polymicro Technologies) that were directly attached to microdrivable system (Lin et al., 2006; Tan et al., 2018). The insulation of the tetrodes to be attached to 36-pin connector array (NPD-36-DD-GS, Omnetics) were removed and then attached via individual soldering to each pin. After soldering of all tetrodes and reference wires (copper wire) to open four pins on end of connectors, epoxy glue was used to immobilize and protect wires (Loctite). The other end of tetrode was pushed through polyamide tubing, then secured by glue when in desired position.

To implant tetrodes, mice were anaesthetized with ketamine/xylazine (0.1 ml/10 g bodyweight, i.p.; Sigma), then head shaved before immobilizing in stereotaxic apparatus (model 38528, RWD Life Science Co). The scalp was treated with betadine solution before being removed and exposing the skull. The skull was then cleaned with 1% hydrogen peroxide to expose suture lines so that they could be easier to observe and identify bregma. The dorsal hippocampus (dHPC; 2.0 mm anterior, 1.5 mm lateral, 1.15 mm ventral) was identified and a circular 1-mm diameter burr hole made in the skull. Before the removal of the dura, five

screws were implanted around the burr hole, including one in the center of the cerebellum that was used to attach the reference via soldering (Gillespie et al., 2016; Fox et al., 2017; Tan et al., 2018; Oliva et al., 2020). The electrode for surgical implantation was more dorsal to the intended region in order that the electrodes might be advanced to location before recording. Animals were allowed one week postsurgery to recover. Before recording, tetrodes were advanced down until SW-Rs were readily observable during periods of immobility (Fig. 6C, Fig. 7B). *Post hoc* histologic verification was done to ensure recording location, especially anterior-posterior and medial-lateral positioning of electrodes.

In vivo recording

Neuronal activity was recorded by OmniPlex Neural Recording Data Acquisition System, while animal location and movement were recorded from by CinePlex Behavioral Research System (both Plexon Inc.). Signals were amplified and local FPs (LFPs) sampled at 1 kHz and digitally filtered between 0.5 and 500 Hz. Spikes were detected using an adjustable online thresholding system that when triggered sampled spikes at 40 kHz. Offline, spikes were sorted by first loading into MClust (MClust-4.4; Redish and Schmitzer-Torbert, 2002) and specifically sorted using the unsupervised clustering algorithm KlustaKwik (Harris et al., 2000). Spikes were sorted for energy, peak and valley (Spellman et al., 2015; Tan et al., 2018), then verified by visual inspection, interspike interval (ISI) distribution and isolation distance (Harris et al., 2001; Schmitzer-Torbert and Redish, 2004; Schmitzer-Torbert et al., 2005; Fox et al., 2017).

Electromyography (EMG) recording, sleep recording, and sleep bout classification

After electrode insertion (see above), insulated wires were inserted into the neck musculature, where wire endings were exposed at the end (Ma et al., 2019; Zhong et al., 2019). Muscle electrodes were immobilized by attachment to skull and headcaps described previously. Animals were recorded during light phase in 2- to 4-h increments at least once during each the morning, afternoon and evening. Sleep states were analyzed by converting LFP and EMG recordings to .EDF before being loaded into Sirenia Sleep Pro 2.1.1 (Pinnacle Technology Inc). Sleep bouts were analyzed in 10 s bouts by taking a fast Fourier transform (FFT) with a Hann window, where wake states was classified when EMG was above threshold, NREM states when EMG was below threshold and δ frequency (0.5–4 Hz) was high and θ frequency (4–12 Hz) and REM states when δ frequency was low and θ frequency high (Levenga et al., 2018).

Waveform analysis and firing rate

All analysis were performed in MATLAB (MathWorks) with custom written scripts. Sorted units were averaged across tetrodes and then calculated for two measures to assess the size of the waveform that is the half-valley width and the width from trough to peak (Mizuseki et al., 2011; Stark et al., 2013; Fox et al., 2017). Waveforms for each neuron were then taken and clustered using a Gaussian mixture model ($k=2$). Those clustered in the group with smaller wave were called “putative INs,” whereas those with clustered into larger waveforms “putative PyNs” (Stark et al., 2013; Spellman et al., 2015). Burst analysis was performed by investigating the ISI 20-ms around SW-R events in 0.5-ms bins with a Gaussian filter of 1.5 ms.

SW-R analysis

For both *in vitro* and *in vivo* signals were loaded into MATLAB (abfload <https://github.com/fcollman/abfload> *in vitro*, Neuroexplorer-Plexon Inc. *in vivo*). For *in vivo*, SW-Rs were detected offline and channel was chosen with largest ripple amplitude and SW-R could be observed on all other wires of the tetrode (Csicsvari et al., 1999; Cheng and Frank, 2008; Jadhav et al., 2012; Kay et al., 2016; Nitzan et al., 2020). For *in vivo*, signals were filtered between 150 and 250 Hz using a fourth order Butterworth filter (Nitzan et al., 2020). An envelope from the signal root mean square using a 4-ms sliding window was calculated and upper envelope taken (Csicsvari et al., 1999; Cheng and Frank, 2008; Jadhav et al., 2012; Kay et al., 2016; Nitzan et al., 2020). Signals from the upper envelope was taken as the ripple envelope for signals larger than 3 SDs above

mean lasting longer than 15-ms (Karlsson and Frank, 2009; Gillespie et al., 2016; Kay et al., 2016; Rothschild et al., 2017). For *in vitro* SW-R detection, signals were filtered between 1 and 50 Hz using a second order Butterworth filter, then taking the envelope from the root mean square as the ripple envelope, where events 3–4 SDs above the mean lasting longer than 15 ms were extracted as SW-R events (Maier et al., 2011; Norimoto et al., 2012, 2013, 2018; Schlingloff et al., 2014; Caccavano et al., 2020).

For *in vitro* SW-R analysis, sharp wave amplitude was the peak of events from the 1- to 50-Hz filtered frequency. For the size of SW-R events for both *in vitro* and *in vivo*, the size of SW-R events were considered those that before above the mean, once the threshold was crossed (Cheng and Frank, 2008; Karlsson and Frank, 2009; Carr et al., 2012). The power of ripples events were the squared signal from SW-R events in the 100- to 300-Hz filtered (as previous) frequency range. For power spectrum density (PSD) plots, PSD quantification, PSD event triggered quantification and event-triggered heatmaps, the MATLAB toolbox *Chronux* (<http://chronux.org>; Gillespie et al., 2016) was used. For all calculations, the time-bandwidth was three and tapers five (*Chronux* default).

Software accessibility

Custom MATLAB code is available on request for any and all code used for previously described analysis.

Immunohistochemistry and confocal imaging

Adult male mice (two months, either wild-type or T796G) were anesthetized with isoflurane perfused transcardially with 0.1 M PBS (pH 7.4). After blood flushed, 4% paraformaldehyde (PFA) dissolved in the same PBS were perfused. Brains were removed and postfixed in 4% PFA for 6–8 h. Coronal sections were cut on a vibratome (50 μ m, Leica VT1000S). Slices were then switched to Tris base saline (0.05 M TBS, pH 7.2). Slices were first permeabilized with 0.5% Triton X-100 in TBS for 1 h. Slices were then blocked via incubation in 10% donkey serum albumin solution in permeabilization solution for 1.5–2 h at 4°C. Primary antibodies were made with blocking solution anti-PV (1:1000, Synaptic Systems, polyclonal) and anti-Neun (1:1000, EMD Millipore, monoclonal). Slices were incubated with primary antibody for 24 h at 4°C. Secondary antibodies (1:500, Jackson ImmunoResearch) were incubated in blocking solution (5% donkey serum albumin) for 2 h at room temperature, then incubated for 10 min with DAPI (1:1000) before mounting with aqueous mounting solution (Aqua-Mount Lerner Laboratories, Thermo Fisher Scientific).

Chemicals and antibodies

Recombinant NRG1 was prepared as previously described (Huang et al., 2000; Woo et al., 2007; Tan et al., 2018). The EGF domain of the β -type NRG1 (rHRG β 177-2444) was prepared as a recombinant polypeptide and prepared as 10 μ M stock in PBS with 1% bovine serum albumin (BSA) in PBS before diluting to 10 nM concentration again with 1% BSA in PBS (Huang et al., 2000). 1NMPP1 was purchased from EMD Sigma (product #529581). Rabbit anti-PV antibody was purchased from Synaptic Systems (product #195004, polyclonal). Mouse anti-Neun antibody was purchased from EMD Millipore (product #MAB377, monoclonal). For slice recording, NRG1 and 1NMPP1 were added the perfusion reservoir of bubbled ACSF. For *in vivo* experiments, 1NMPP1 or DMSO (as control) was injected intraperitoneally at 0.1 μ g/g body weight or delivered consecutively by two osmotic pumps (Model 1004, ALZET) that were implanted in the abdomen. 1NMPP1 was delivered at flow rate 0.11 μ l/h each pump, for a total 0.1 μ g/g body weight every 2 h.

Statistical analysis

Two-tailed paired or un-paired Student's *t* test was used for analyzing data set with two groups, when normality data test (Kolmogorov–Smirnov) was met. When not, nonparametric two-tailed paired (Wilcoxon rank-sum test) and unpaired (Mann–Whitney) were used;

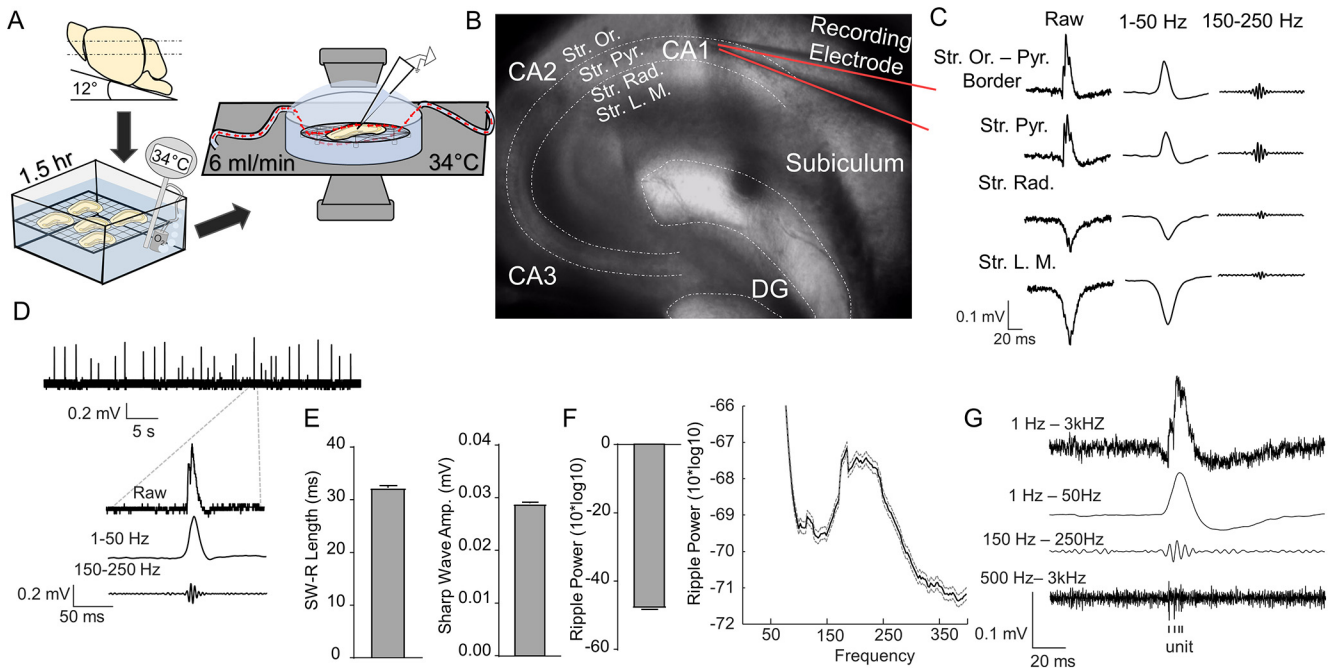


Figure 1. Spontaneously occurring SW-Rs, SW-R laminar validation, and differing SW-R components. **A**, Schematic diagram of recording. **B**, Representative image of a hippocampal slice where an electrode (red) was placed in stratum pyramidal (Str. Pyr.); stratum oriens (Str. Or.); stratum radiatum (Str. Rad.); stratum lacunosum (Str. L.M.). **C**, Laminar profiles of sharp wave ripples (SW-Rs) in the CA1 region. Shown were a representative positive deflection (left) and corresponding sharp wave (middle) and ripples (right) after filtration at 1–50 and 50–250 hertz Hz, respectively. **D**, Representative field potentials (FPs) and SW-Rs. A positive deflection and related SW-Rs were shown in the bottom. **E**, Quantitative analysis of sharp wave length and amplitude. **F**, Ripple power spectrum density (PSD) across ripple frequencies. Averaged ripple power from 150 to 300 Hz was shown in the histogram. **G**, Raw traces (top) from SW-R event filtered sharp wave (1–50 Hz), ripple (150–250 Hz) and single units [500–3 kHz, displaying single unit activity (tick marks)]. Error bars indicate SEM.

$p < 0.05$ is considered significant. Data graphically were represented with mean \pm SEM unless otherwise noted.

Results

NRG1 decreases SW-R occurrence

To determine whether SW-Rs are regulated by NRG1, thick ($\sim 450 \mu\text{m}$) horizontal hippocampal slices were prepared from 4- to 12-week-old mice. Sections were sliced at a 12° angle to preserve hippocampal structures such as the DG, CA1–3 and Schaffer-collateral projections (Fig. 1A), as described previously (Norimoto et al., 2012). Slices were incubated in 34°C , oxygenated ACSF for 1.5 h, and recorded in a dual superfusion chamber perfused with ACSF at 6 ml/min at 34°C (Fig. 1A; Maier et al., 2003; Norimoto et al., 2018). FPs were recorded in different layers of the CA1 region (Fig. 1B,C), which displayed laminar voltage changes characteristic of SW-Rs (Buzsáki, 1986; Ylinen et al., 1995; Maier et al., 2003). In particular, there were positive deflections in the stratum oriens and stratum pyramidale, but negative deflections in the stratum radiatum and stratum lacunosum border (Maier et al., 2003, 2009). Filtering FPs by 1–50 Hz generated sharp waves with durations of >15 ms and amplitudes of 3–4 SD above the baseline (Fig. 1D). On average, the duration of sharp waves was 32.2 ± 0.44 ms and amplitudes of 0.03 ± 0.002 mV (Fig. 1E), in agreement with previous studies (Maier et al., 2003, 2009; Norimoto et al., 2012, 2013, 2018). Within the sharp waves were ripple events, revealed by 150- to 250-Hz filtration (Maier et al., 2003). When the ripple power in each deflection was analyzed, a peak in the PSD was observed around the 150- to 250-Hz range; the averaged ripple power of bandpassed filtered signal between 150 and 250 Hz was -48.1 ± 0.18 $10 \cdot \log_{10}$ (Fig. 1F). As shown in Figure 1G,

sharp-wave and/or ripples were most dominant in the stratum pyramidale. Furthermore, filtering of high-frequency components revealed an increase in units discharging during SW-Rs (Fig. 1G; Maier et al., 2003; Both et al., 2008; Schlinghoff et al., 2014). These characteristics were in agreement with previous reports (Maier et al., 2003; Norimoto et al., 2012, 2018). Unless otherwise indicated, we focused on positive deflections and SW-Rs in the pyramidal layer (Norimoto et al., 2012, 2018; Schlinghoff et al., 2014).

To investigate the impact of NRG1 on SW-Rs, hippocampal slices were treated with NRG1 (at 10 nM, final concentration) as indicated in Figure 2A. Interestingly, NRG1 acutely reduced the frequency of SW-R-containing positive deflections in the pyramidal layer (0.28 ± 0.07 to 0.21 ± 0.07 Hz, $t_{(5)} = 3.25$ $p = 0.02$, paired t test; Fig. 2B,C). This effect was reversible because the SPW-R occurrence after NRG1 washout returned to comparable levels of the pretreatment baseline (0.21 ± 0.07 to 0.27 ± 0.07 Hz, $t_{(5)} = 2.94$ $p = 0.03$, paired t test). These results indicate a role of NRG1 in regulating SW-Rs in the hippocampus. We determined whether NRG1 altered SW-R components. The length of sharp waves after NRG1 treatment were similar to baseline and washout (40.6 ± 2.86 ms for baseline, 46.6 ± 4.87 ms for NRG1, and 41.56 ± 3.25 ms for washout; baseline $t_{(5)} = 1.86$ $p = 0.12$, $t_{(5)} = 2.00$ washout $p = 0.10$, paired t test; Fig. 2D). Next, we measured the amplitude of sharp wave events. As shown in Figure 2E, NRG1 had little effect on the amplitude of sharp waves compared with baseline and washout (0.02 ± 0.002 ms for baseline, 0.02 ± 0.001 mV for NRG1, and 0.02 ± 0.001 ms for washout; base $t_{(5)} = 2.45$ $p = 0.06$, washout $t_{(5)} = 1.20$ $p = 0.28$ paired t test). To determine whether the ripple components were altered by NRG1, we analyzed the ripple power in each deflection against 150- to 250-Hz spectrum. The PSD curves superimposed across the frequencies of the baseline, NRG1 or washout group

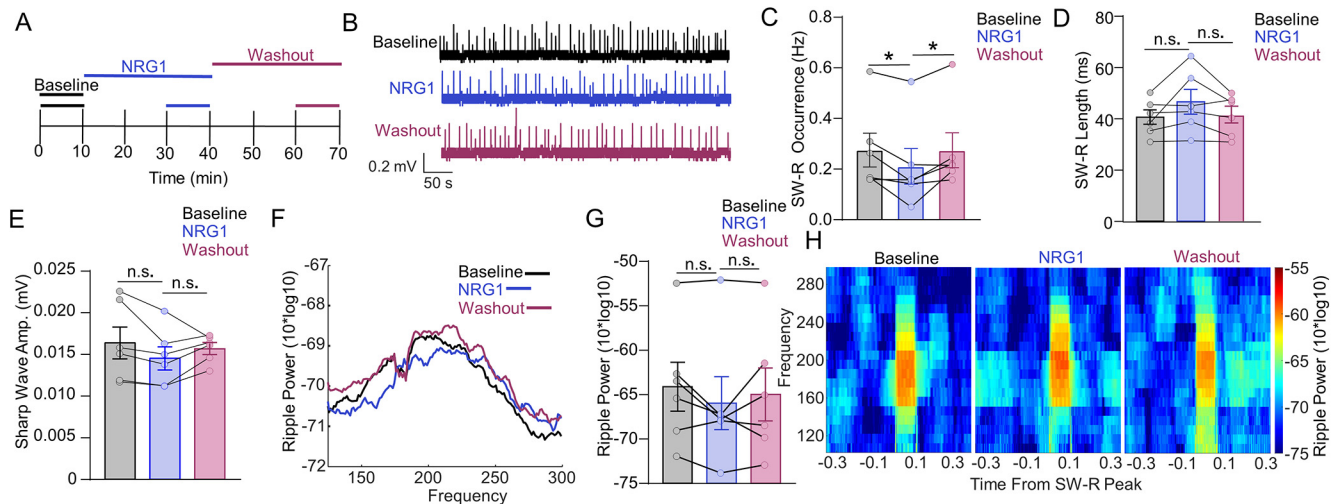


Figure 2. NRG1 decreases SW-R occurrence in wild-type hippocampus *in vitro*. **A**, Neuregulin 1 (NRG1) treatment paradigm. **B**, Representative filed potentials (FPs) in CA1 region at baseline, NRG1 treatment, and washout. **C**, Decreased sharp wave ripple (SW-R) occurrence by NRG1 (10 nM, blue), compared with baseline (black) and washout (purple). **D**, **E**, No effect on sharp wave length (**D**) or amplitude (**E**) by NRG1 (blue), compared with baseline (black) or washout (purple). **F**, Overlapped power spectrum density (PSD) distribution curves across different frequencies. Shown were representative curves of baseline (black), NRG1 (blue), and washout (purple). **G**, No effect of NRG1 on ripple power between 150 and 300 Hz. **H**, Similar heatmap of (PSD) of SW-R events from baseline (left), NRG1 (center), and washout (right; $n = 6$ slices, 6 wild-type mice). Error bars indicate SEM. n.s., not significant. * $p < 0.05$.

displayed similar PSD distributions (Fig. 2*F*). Quantitatively the PSD showed no statistical difference among the three groups (-64.1 ± 2.70 $10 \cdot \log_{10}$ for baseline, -66.0 ± 2.97 $10 \cdot \log_{10}$ for NRG1, and -65.0 ± 2.99 $10 \cdot \log_{10}$ for washout, baseline $t_{(5)} = 1.95$ $p = 0.11$, washout $t_{(5)} = 0.82$ $p = 0.45$, paired t test; Fig. 2*G*). This finding was further supported by heatmaps showing similar ripple power from 100 to 300 Hz of the three different groups (Fig. 2*H*). Together, these results indicate that NRG1 reduces the frequency of SW-Rs without altering characteristic components and reveal a novel mechanism of NRG1 in regulating an important hippocampal function.

Requirement of ErbB4 kinase activity for SW-Rs

Neuronal activity in the hippocampus is regulated by homeostatic NRG1-ErbB4 activity (Mei and Xiong, 2008; Mei and Nave, 2014). In particular, neutralizing endogenous NRG1 or inhibiting ErbB4 reduces GABA release, impairs synaptic plasticity and alters behaviors in mice (Li et al., 2007; Fazzari et al., 2010; Del Pino et al., 2013, 2017; Tan et al., 2018). Therefore, we determined whether SW-Rs are altered by pharmacological inhibition of ErbB4. To this end, hippocampal slices were treated with 10 μ M PD168393, an inhibitor that is relatively specific for ErbB4 among receptor tyrosine kinases (Koprivica et al., 2005). SW-Rs were analyzed before and 20 min after the addition of PD168393 as shown in Figure 3*A*. Interestingly, the frequency of SW-R-containing positive deflections was increased by PD168393 (from 0.36 \pm 0.09 to 0.43 \pm 0.09 Hz, $t_{(7)} = 4.43$ $p = 0.003$, paired t test; Fig. 3*B,C*). These results reveal a novel regulatory mechanism of SW-Rs. However, PD168393 had little effect on the length of SW-Rs (43.5 \pm 3.14 ms for baseline, 44.2 \pm 2.97 ms for PD168393, $t_{(7)} = 0.29$ $p = 0.78$, paired t test; Fig. 3*D*), or the amplitude of sharp waves (0.02 \pm 0.003 mV for baseline, 0.03 \pm 0.004 mV for PD168393, $t_{(7)} = 0.84$ $p = 0.43$, paired t test; Fig. 3*E*). Lastly, we investigated whether PD168393 altered the ripple power. As quantified in Figure 3*F*, PD168393 had no effect on the ripple power (-65.9 ± 2.95 $10 \cdot \log_{10}$ for baseline, -65.1 ± 3.50 $10 \cdot \log_{10}$ for PD168393, $t_{(7)} = 0.99$ $p = 0.36$, paired t test; Fig. 3*F*). Together, these results suggest a

role of ErbB4 in regulating the frequency of SW-Rs without altering characteristic components.

To further test this hypothesis, we studied SW-Rs in a chemical genetic mutant strain of ErbB4, T796G mice (Tan et al., 2018). In T796G mice, the ATP binding pocket of ErbB4 was enlarged by mutating threonine 796 (T796) to glycine that allows for access by the bulky inhibitor 1NMPP1 (Fig. 4*A*; Bishop et al., 2000). Unlike ErbB4 null mice that die at embryonic stages because of cardiac deficits, T796G mice are viable with similar gross anatomic structures in the brain (Gassmann et al., 1995; Tan et al., 2018). The hippocampal organization or the number of PV+ and NeuN+ cells were similar to those of wild-type mice (Fig. 4*B–D*; PV, 87.7 \pm 2.60 cells per μ m² for wild type, 83.9 \pm 5.48 cells per μ m² for T796G, $t_{(10)} = 0.63$ $p = 0.54$, unpaired t test, NeuN, 1238 \pm 156 cells per μ m² for wild type, 1263 \pm 100 cells per μ m² for T796G, $t_{(12)} = 0.14$ $p = 0.89$, unpaired t test; Tan et al., 2018). SW-Rs recorded in T796G hippocampal slices were similar to those in wild-type slices including SW-R occurrence rate (0.35 \pm 0.05 Hz for wild type, 0.33 \pm 0.04 Hz for T796G, $t_{(11)} = 0.30$ $p = 0.88$, unpaired t test; Fig. 4*E*), the length of SW-Rs (44.7 \pm 1.95 ms for wild type, 44.8 \pm 2.33 ms for T796G, $t_{(11)} = 0.03$ $p = 0.97$, unpaired t test; Fig. 4*F,G*) amplitudes of sharp waves (0.02 \pm 0.002 mV for wild type, 0.02 \pm 0.002 mV for T796G, $t_{(11)} = 0.15$ $p = 0.88$, unpaired t test; Fig. 4*H*) and ripple power (-65.4 ± 1.44 $10 \cdot \log_{10}$ for wild type, -65.0 ± 1.88 $10 \cdot \log_{10}$ for T796G, $t_{(11)} = 0.14$ $p = 0.89$, unpaired t test; Fig. 4*I*). These data indicate that the T796G mutation has no effect on hippocampal structure or SW-R production.

We showed previously that 1NMPP1 was able to acutely inhibit ErbB4 kinase activity in the brain of T796G mice and reduces GABA release in hippocampal slices (Tan et al., 2018). To specifically inhibit ErbB4, hippocampal slices of T796G mice were treated with 1NMPP1 (Fig. 3*G*). As shown in Figure 3*H*, SW-R occurrence increased by 1NMPP1; the increase returned to baseline levels after washout, indicating that the effect is reversible (baseline, 0.30 \pm 0.07 Hz; 1NMPP1, 0.36 \pm 0.06 Hz, washout, 0.30 \pm 0.07 Hz, baseline $t_{(5)} = 3.00$ $p = 0.03$, washout

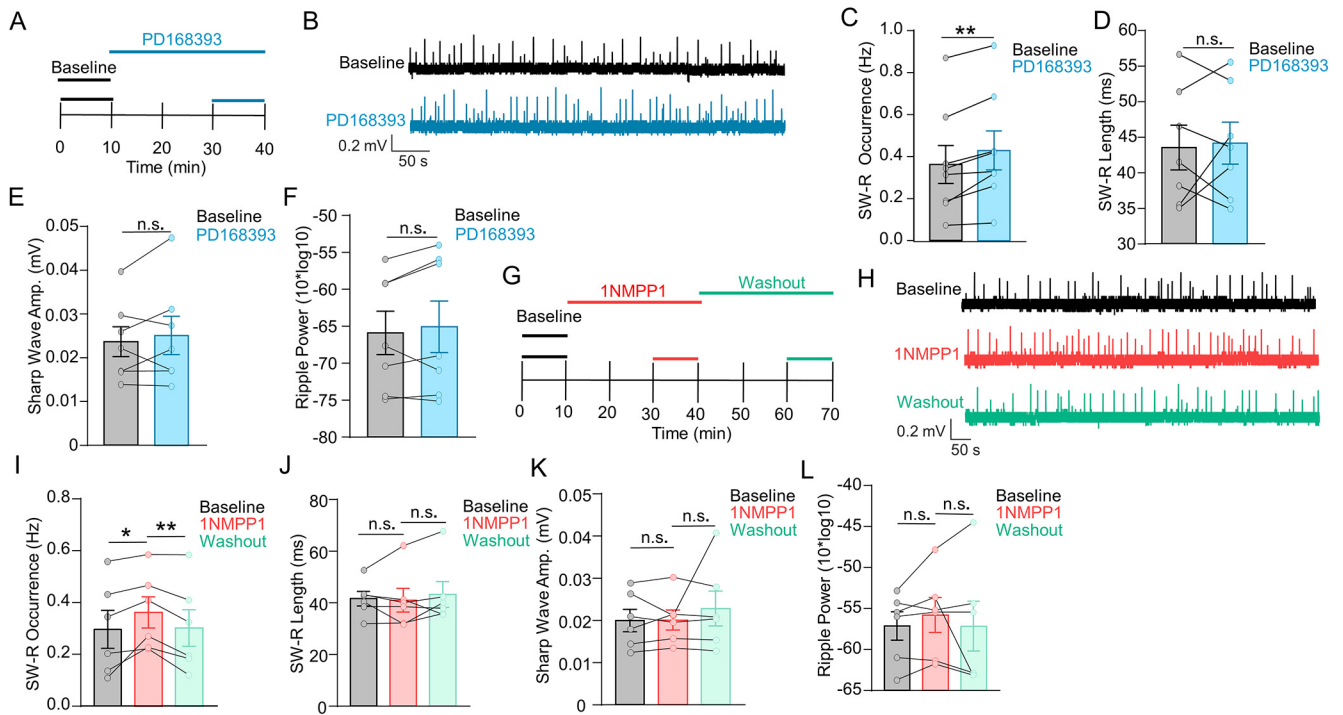


Figure 3. Blocking endogenous ErbB4 kinase increases SW-R occurrence. **A**, PD168393 treatment paradigm. **B**, Representative filled potentials (FPs) in CA1 region at baseline and PD168393 treatment. **C**, Increased SW-R occurrence by PD168393 (blue, 10 μ M) compared with baseline (black). **D**, **E**, No effect on sharp wave length (**D**) or amplitude (**E**) by PD168393 (blue), compared with baseline (black). **F**, No effect of PD168393 (blue) on ripple power between 150 and 300 Hz ($n = 7$ slices, 7 wild-type mice). **G**, 1NMPP1 treatment paradigm of T796G hippocampal slices. **H**, Representative FPs in CA1 region at baseline, 1NMPP1 treatment and washout. **I**, Increased SW-R occurrence by 1NMPP1 (10 μ M, red), compared with baseline (black) and washout (green). **J**–**L**, No effect on sharp wave length (**J**) or amplitude (**K**) by 1NMPP1 (red), compared with baseline (black) or washout (green). **L**, No effect of 1NMPP1 on ripple power between 150 and 300 Hz ($n = 6$ slices, 6 T796G mice). Error bars indicate SEM. n.s., not significant. * $p < 0.05$. ** $p < 0.01$.

$t_{(5)} = 4.19$ $p = 0.01$, paired t test; Fig. 3I). These results provide compelling evidence for a role of dynamic ErbB4 kinase activity in regulating SW-Rs. As observed for PD168393, SW-R length was not altered by 1NMPP1 (41.6 ± 2.79 ms for baseline, 41.0 ± 4.54 ms for 1NMPP1, 43.2 ± 5.02 , baseline $t_{(5)} = 0.25$ $p = 0.81$, washout $t_{(5)} = 1.10$ $p = 0.32$, paired t test; Fig. 3J). Furthermore, no change was observed in the amplitude of sharp waves after 1NMPP1 administration (0.02 ± 0.002 mV for baseline, 0.02 ± 0.002 mV for 1NMPP1, 0.02 ± 0.004 mV, baseline $t_{(5)} = 0.09$ $p = 0.93$, washout $t_{(5)} = 0.81$ $p = 0.45$, paired t test; Fig. 3K) nor did 1NMPP1 have any effect on the ripple power (-57.2 ± 1.72 $10 \cdot \log_{10}$ for baseline, -55.8 ± 2.13 $10 \cdot \log_{10}$ for 1NMPP1, -57.2 ± 3.02 $10 \cdot \log_{10}$, baseline $t_{(5)} = 0.77$ $p = 0.18$, washout $t_{(5)} = 1.56$ $p = 0.48$, paired t test; Fig. 3L). These results support a model that dynamic ErbB4 activity is necessary for normal exhibition of SW-Rs.

Requirement of ErbB4 activity for NRG1 regulation of SW-R

The increase in SW-R occurrence by acute treatment with PD168393 and 1NMPP1 suggests an important role of endogenous NRG1-ErbB4 activity in regulating SW-Rs. To further test this hypothesis, we next determined whether NRG1 suppression of SW-Rs requires ErbB4 activity. NRG1 reduced the frequency of SW-R-containing positive deflections in T796G hippocampal slices; however, this effect was blocked by 1NMPP1 (baseline, 0.36 ± 0.04 Hz; NRG1, 0.22 ± 0.05 , NRG1 + 1NMPP1, 0.34 ± 0.03 Hz, washout, 0.35 ± 0.03 Hz, baseline-NRG1 $t_{(18)} = 2.34$ $p = 0.03$, baseline-NRG1 + 1NMPP1 $t_{(20)} = 0.40$ $p = 0.69$, NRG1-washout $t_{(18)} = 2.54$ $p = 0.02$, NRG1-NRG1 + 1NMPP1 $t_{(12)} = 2.15$ $p = 0.05$, unpaired t test; Fig. 5A), indicating that NRG1 regulates SW-R occurrence by activating ErbB4. As observed in

Figure 2, NRG1 had no effect on the length of SW-Rs, the amplitude of sharp waves, or the ripple power in wild-type mice. Similarly, these parameters (except the SW-R frequency) were not altered by 1NMPP1 in T796G mice (Fig. 3). Likewise, we did not observe a difference between baseline, NRG1, NRG1 + 1NMPP1 or washout in the length of sharp waves (baseline, 44.1 ± 3.25 ms, NRG1, 49.7 ± 6.79 ms, NRG1 + 1NMPP1, 40.4 ± 2.02 ms, washout, 44.8 ± 3.98 ms, baseline-NRG1 $t_{(18)} = 0.85$ $p = 0.41$, baseline-NRG1 + 1NMPP1 $t_{(20)} = 0.80$ $p = 0.44$, NRG1-washout $t_{(18)} = 0.65$ $p = 0.53$, NRG1-NRG1 + 1NMPP1 $t_{(12)} = 1.48$ $p = 0.16$, unpaired t test; Fig. 5B), the amplitude (baseline, 0.02 ± 0.001 mV, NRG1, 0.02 ± 0.002 mV, NRG1 + 1NMPP1, 0.02 ± 0.001 mV, washout, 0.02 ± 0.01 mV, baseline-NRG1 $t_{(18)} = 0.22$ $p = 0.83$, baseline-NRG1 + 1NMPP1 $t_{(20)} = 0.21$ $p = 0.84$, NRG1-washout $t_{(18)} = 0.03$ $p = 0.97$, NRG1-NRG1 + 1NMPP1 $t_{(12)} = 0.05$ $p = 0.96$, unpaired t test; Fig. 5C), or the ripple power (baseline, -60.7 ± 1.78 $10 \cdot \log_{10}$, NRG1, -58.5 ± 3.78 $10 \cdot \log_{10}$, NRG1 + 1NMPP1, -62.8 ± 1.43 $10 \cdot \log_{10}$, washout, -60.8 ± 1.78 $10 \cdot \log_{10}$, baseline-NRG1 $t_{(18)} = 0.61$ $p = 0.55$, baseline-NRG1 + 1NMPP1 $t_{(20)} = 0.79$ $p = 0.441$, NRG1-washout $t_{(18)} = 0.64$ $p = 0.53$, NRG1-NRG1 + 1NMPP1 $t_{(12)} = 1.18$ $p = 0.262$, unpaired t test; Fig. 5D). Together, these results demonstrate that NRG1 reduces the frequency of SW-Rs in a manner that requires ErbB4 kinase activity.

1NMPP1 increases SW-R occurrence *in vivo*

To determine whether SW-Rs require ErbB4 kinase activity *in vivo*, we examined 1NMPP1's effect on SW-Rs in freely moving mice. Tetrodes were implanted into the dHPC as described previously (Tan et al., 2018; Fig. 6A). Filtering LFPs at 150–250 Hz revealed ripples that exceeded 3 SDs above baseline mean and

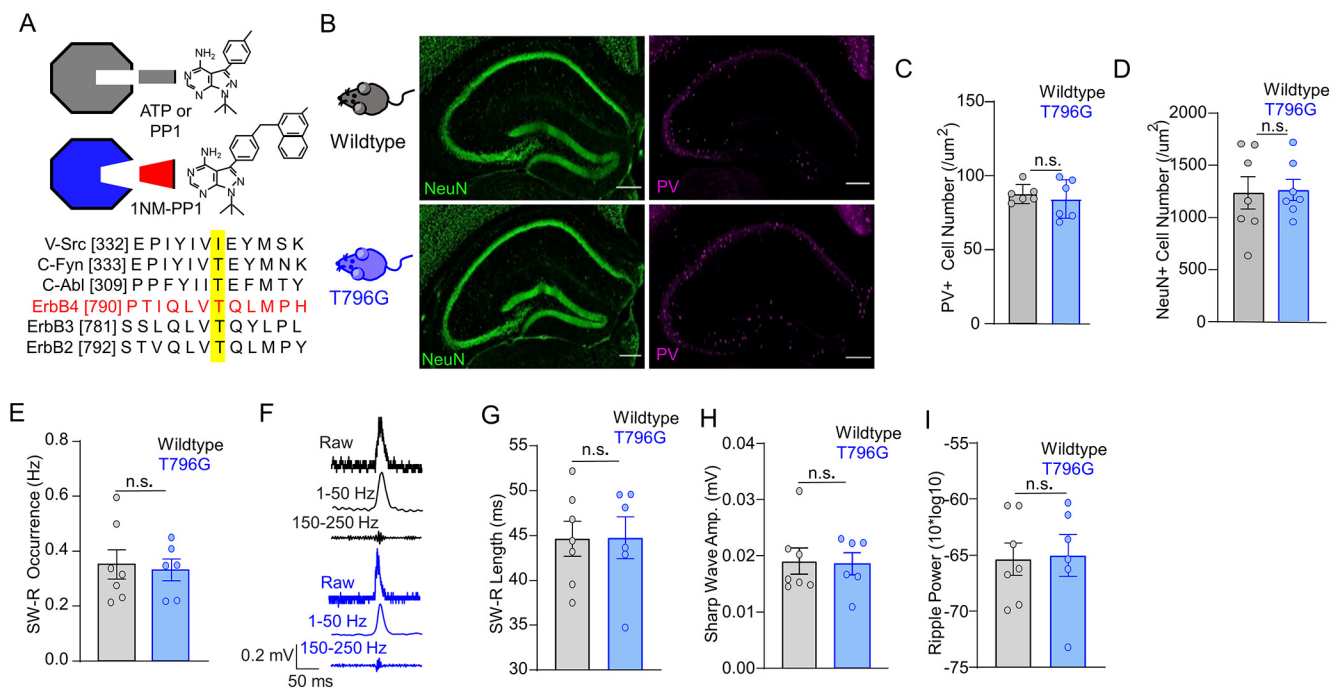


Figure 4. Normal NeuN+ and PV+ cells and SW-Rs in T796G mice. **A**, Cartoon of enlarged ATP binding pocket by T796G mutation (left, bottom) compared with wild-type (left, top). T796 is conserved among indicated kinases (yellow) and targeted for mutation to glycine. **B**, No global changes in global structure and neuron numbers. Hippocampus of wild-type and T796G mice were stained for NeuN (green, left) and PV (purple, right). **C**, Quantification of **A**, **B** PV immunohistochemistry per μm^2 . No alteration between wild-type [black, $n = 6$ slices (3 animals)] and T796G [blue, $n = 6$ slices (3 animals)]. **D**, Quantification of **A**, **B** NeuN immunohistochemistry per μm^2 . No alteration between wild-type [black, $n = 6$ slices (3 animals)] and T796G [blue, $n = 6$ slices (3 animals)]. **E**, No difference between sharp wave ripple (SW-R) occurrence in wild-type (black) and T796G (blue) mice. **F**, Example SW-R traces from wild-type (black) and T796G (blue) recordings. **G–I**, No difference of sharp wave length (**G**), amplitude (**H**), and ripple power (**I**) between wild-type (black) and T796G [blue; wild-type $n = 7$ slices (7 mice), T796G $n = 6$ slices (6 mice)]. Error bars indicate SEM. n.s., not significant.

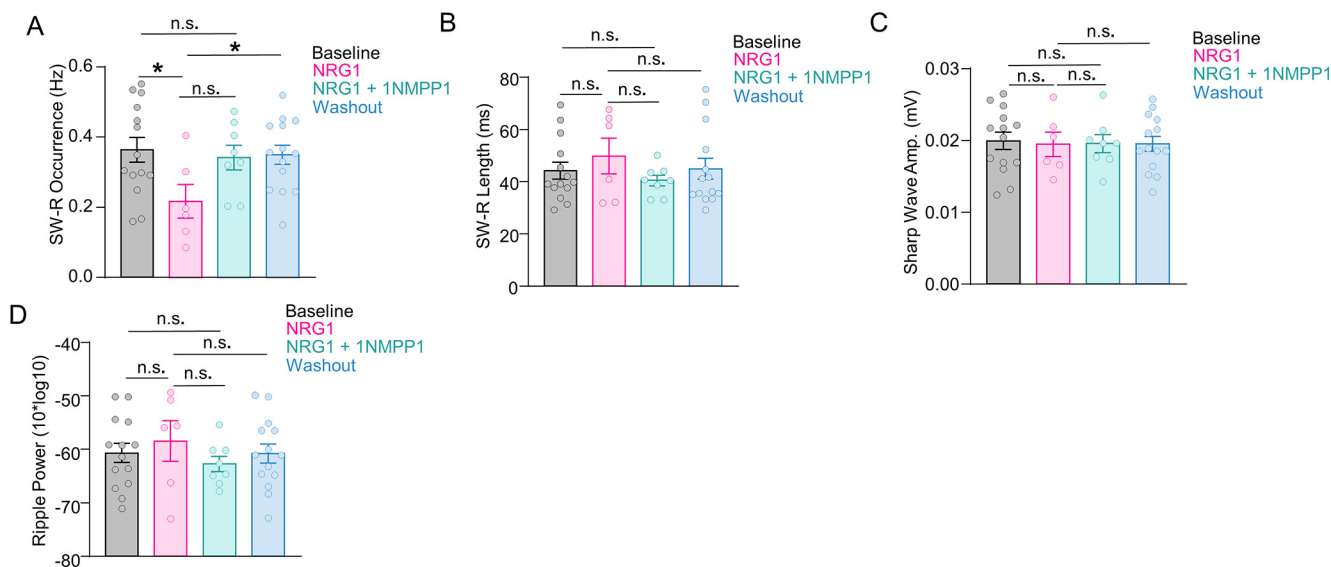


Figure 5. 1NMPP1 blocks NRG1 dependent decrease in SW-R occurrence in the CA1 hippocampus *in vitro*. **A**, Inability of Neuregulin 1 (NRG1) to decrease SW-R occurrence in presence of 1NMPP1 in T796G slices. **B**, **C**, No effect on sharp wave length (**B**) or amplitude (**C**) by NRG1 (pink) or NRG1 + 1NMPP1 (green), compared with baseline (black) or washout (green). **D**, No effect of NRG1 (pink) or NRG1 + 1NMPP1 (green) on ripple power between 150 and 300 Hz compared with baseline (black) or washout (green; NRG1 $n = 6$ slices, 6 T796G mice; NRG1 + 1NMPP1 $n = 8$ slices, 8 T796G mice). Error bars indicate SEM. n.s., not significant. * $p < 0.05$.

persisted for >15 ms (Karlsson and Frank, 2008; Carr et al., 2012; Kay et al., 2016). These ripple events were readily detectable during immobility (Fig. 7B). Because *in vivo* ripples are influenced by novelty (such as novel environments; Karlsson and

Frank, 2009; Fernández-Ruiz et al., 2019), we habituated mice to an enclosed chamber with bedding (Figs. 6A, 7A) for 1 h/d for 5 d and to injection procedure with vehicle at days 6 and 7 (Fig. 7A; Gillespie et al., 2016). LFPs were recorded on day 8, 20 min

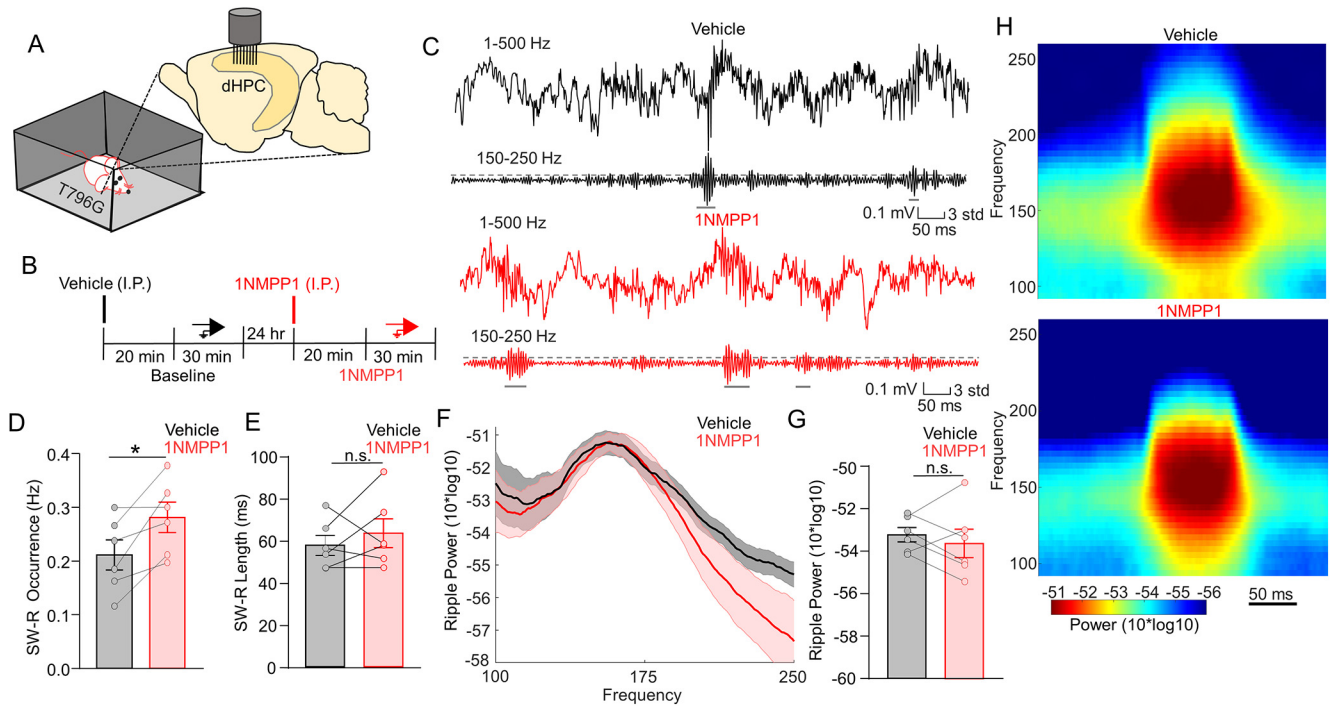


Figure 6. 1NMPP1 increases SW-R occurrence in the dHPC CA1 *in vivo*. **A**, Schematic of electrode implantation and recording. Tetrodes were implanted into the dorsal hippocampus (dHPC) of T796G mice. **B**, Schematic of treatment and recording paradigms. **C**, Example traces of raw LFP (1–500 Hz, top) and ripples after filtering at 150–250 Hz (bottom). **D**, Increased SW-R occurrence by 1NMPP1 (red) compared with vehicle (black). **E**, No effect on SW-R length by 1NMPP1 (red) compared with vehicle (black). **F**, Overlapped power spectrum density (PSD) distribution curves across different frequencies. **G**, No effect by 1NMPP1 (red) compared with vehicle (black) on SW-R power. **H**, PSD heatmap of SW-R events from vehicle (top) and 1NMPP1 (bottom). Error bars indicate SEM. n.s., not significant. * $p < 0.05$.

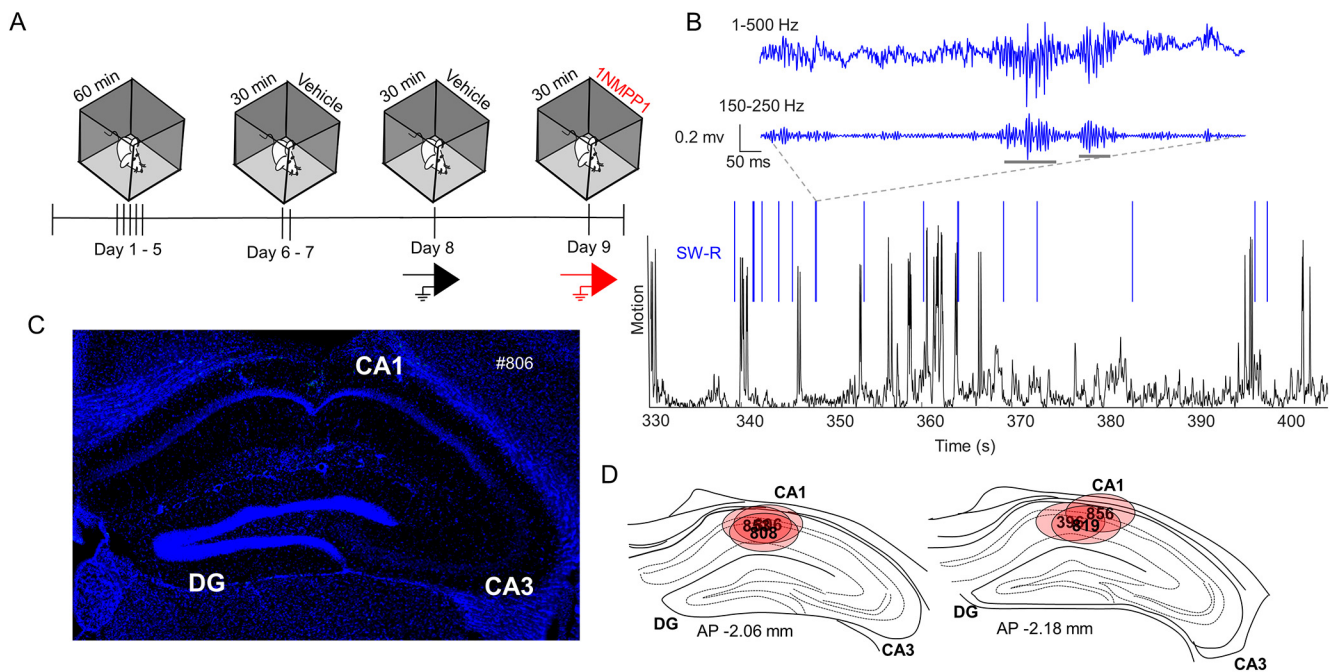


Figure 7. Habituation protocol, validation of SW-R detection and electrode location. **A**, Schematic diagrams of habituation and recording. **B**, Example traces of animal motion (top, black) and sharp wave ripple (SW-R) events during periods of immobility (bottom, blue). Expanded traces (above) displaying events shown in blue marks (below). **C**, **D**, Electrode locations (red) and animal in number (black).

after vehicle injection and on day 9, 20 min after 1NMPP1 (0.1 $\mu\text{g/g}$), at a dosage previously shown to inhibit ErbB4 phosphorylation and disrupt top-down attention (Fig. 6B; Tan et al., 2018). Remarkably, 1NMPP1 increased the occurrence of ripples

(0.21 ± 0.03 Hz for vehicle, 0.28 ± 0.03 Hz for 1NMPP1, $t_{(5)} = 3.13$ $p = 0.03$, paired t test; Fig. 6C,D). Note that 1NMPP1 had no effect on baseline (0.01 ± 0.001 mV for vehicle, 0.01 ± 0.001 for 1NMPP1, $t_{(5)} = 1.29$ $p = 0.26$, paired t test; Fig. 8A) or SD of

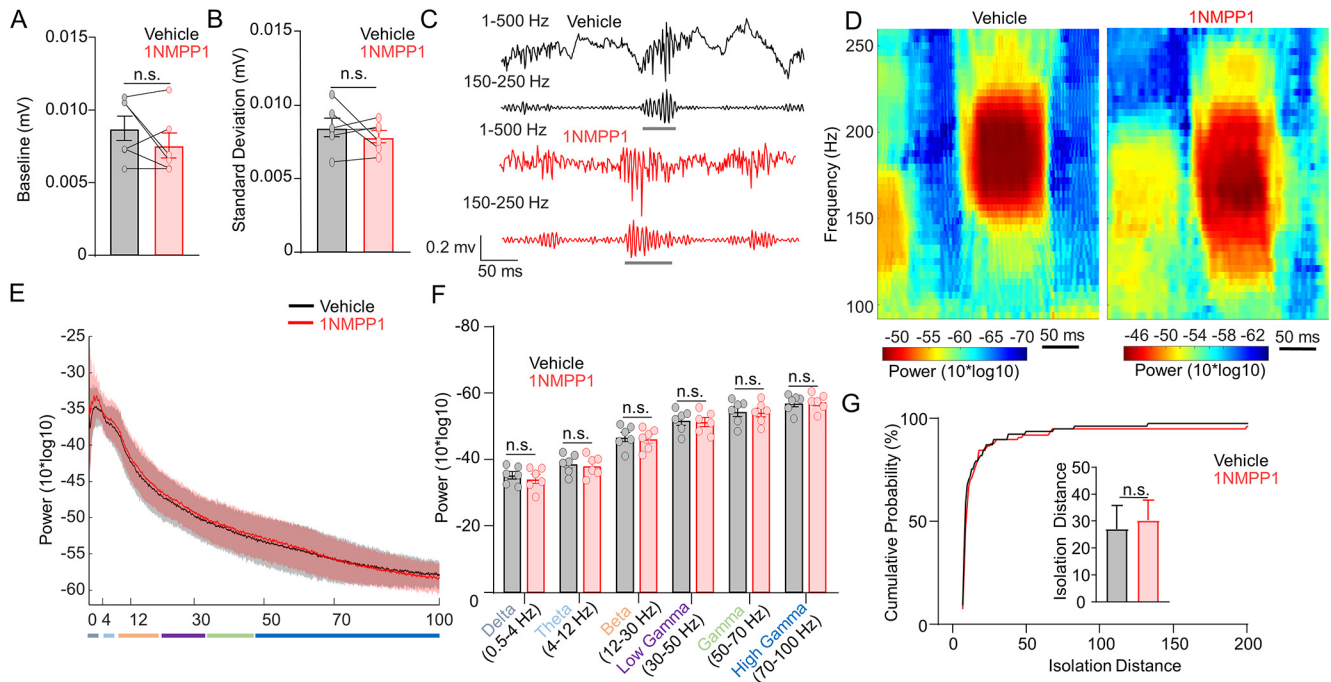


Figure 8. Unaltered dHPC PSD, baseline, SD, and isolation distance after 1NMPP1. **A**, No alteration of 1NMPP1 (red) compared with vehicle (black) on baseline voltage. **B**, No alteration of 1NMPP1 (red) compared with baseline (black) on SD. **C**, Example traces of raw local field potential (LFP) (1–500 Hz, top) and ripple filtered LFP (150–250 Hz, bottom, gray sharp wave ripple (SW-R)) of vehicle (black, top) and 1NMPP1 (red, bottom). **D**, Example SW-R event heatmap from baseline (black) compared with 1NMPP1 (red). **E**, power spectrum density (PSD) ($10 \cdot \log_{10}$) per frequency (1–100 Hertz, Hz) of baseline (black) and 1NMPP1 [red; $n = 6$ recordings (6 T796G mice)]. **F**, Quantification of **E**. No effect of 1NMPP1 (red) compared with baseline (black) on delta (magenta, 0.5–4 Hz), theta (light-blue, 4–12 Hz), beta (orange, 12–30 Hz), low gamma (purple, 30–50 Hz), gamma (green, 50–70 Hz), high gamma [blue, 70–100 Hz; $n = 6$ recordings (6 T796G mice), paired t test, delta: $n.s. = 0.7953$; theta: $n.s. = 0.4395$; beta: $n.s. = 0.7590$; low gamma: $n.s. = 0.4198$; gamma: $n.s. = 0.3137$; high gamma: $n.s. = 0.0881$; $n = 6$ animals, 6 recordings vehicle, 6 1NMPP1]. **G**, Cumulative probability distribution percentage of isolation distance. No effect of 1NMPP1 (red) compared with vehicle (black) on isolation distance red of single units from Figure 6 (27.0 ± 8.691 Hz for vehicle, 30.1 ± 7.63 Hz for 1NMPP1, $U = 3363$ $p = 0.32$, Mann–Whitney test). Error bars indicate SEM. *n.s.*, not significant.

the threshold (0.01 ± 0.001 mV for vehicle, 0.01 ± 0.0004 for 1NMPP1, $t_{(5)} = 0.93$ $p = 0.40$, paired t test; Fig. 8B). This result was in agreement with *in vitro* data, and together, it indicates a role of ErbB4 kinase in regulating ripple number. This effect appeared to be specific because the ripple length was comparable between the groups of 1NMPP1 and vehicle (57.6 ± 4.74 ms for vehicle, 63.3 ± 6.87 for 1NMPP1, $t_{(5)} = 0.84$ $p = 0.44$, paired t test; Figs. 6E, 8C), suggesting a dispensable role of ErbB4 kinase. Furthermore, 1NMPP1 had little effect on PSD distribution across frequencies and ripple-triggered heatmaps from individual recording sessions (-53.2 ± 0.34 $10 \cdot \log_{10}$ for vehicle, -53.6 ± 0.67 $10 \cdot \log_{10}$ for 1NMPP1, $t_{(5)} = 0.73$ $p = 0.49$, paired t test; Figs. 6F–H, 8D).

SW-Rs are believed to be generated by neurons critical to learning and memory, we next investigated whether 1NMPP1 alters the firing of INs and PyNs during SW-R events. PyNs and INs were differentiated by analyzing waveform characteristics: half-valley width and trough-to-peak width (Fig. 9A). Neurons with larger half-valley width and larger trough-to-peak width were clustered as PyNs, in contrast to INs based on clustering using a Gaussian mixture model (Mizuseki et al., 2009; Stark et al., 2014; Fig. 9B). The autocorrelogram (the correlation of spike frequency plotted in both positive and negative directions) showed that PyNs displayed a peak with smaller correlation in time (~ 5 ms), consistent with the bursty firing property of PyNs (Fig. 9C, top panel). In contrast, INs lack a peak within the 5-ms window but with high levels of correlation outside the window, consistent with continuous firing of INs (Fernández-Ruiz et al., 2017, 2021; Oliva et al., 2018). These results validate the clustering of PyNs and INs. As shown in Figure 9D, the overall firing

rate of all neurons was increased by 1NMPP1, compared with vehicle (3.27 ± 0.38 Hz for vehicle, 4.31 ± 0.41 Hz for 1NMPP1, $U = 2968$ $p = 0.026$, Mann–Whitney test). Neuron type analysis indicated that 1NMPP1 had little effect on the firing rates of INs (3.34 ± 0.74 Hz for vehicle, 4.05 ± 0.62 Hz for 1NMPP1, $U = 752$ $p = 0.23$, Mann–Whitney test; Fig. 9E). In contrast, it increased baseline PyN firing (Fig. 9F; 3.26 ± 0.36 Hz for vehicle, 4.64 ± 0.48 Hz for 1NMPP1, $U = 601$ $p = 0.01$, Mann–Whitney test). Intriguingly, 1NMPP1 had little effect on the firing rate of PyNs during SW-Rs (38.3 ± 1.74 Hz for vehicle, 38.6 ± 2.08 Hz for 1NMPP1, $U = 865$ $p = 0.88$, Mann–Whitney test; Fig. 9G). To determine whether 1NMPP1 alters the temporal dynamics of PyN firing during SW-Rs, we investigated the PyN bursting across different ISI during SW-Rs to identify ISI maximal probability (Fig. 9H). Remarkably, it was reduced by 1NMPP1 (Fig. 9I). In addition, the fold change of PyN firing rates during SW-R events were reduced by 1NMPP1 (Fig. 9J). These results suggest that ErbB4 activity is necessary for temporal dynamics of PyN spikes.

Differential effects by 1NMPP1 on SW-R occurrence in NREM and wake states

Next, we investigated effects of 1NMPP1 on SW-Rs at different functional states. SW-Rs occur preferably during NREM states (Buzsáki, 2015) or immobile periods of wake states (Karlsson and Frank, 2009). Therefore, we compared SW-R occurrence between NREM and wake states which were determined by EMG of neck muscles (Fig. 10A). NREM states were classified as epochs where EMG activity was low and dHPC LFP δ frequency (0.5–4 Hz) high whereas wake states as epochs with high EMG

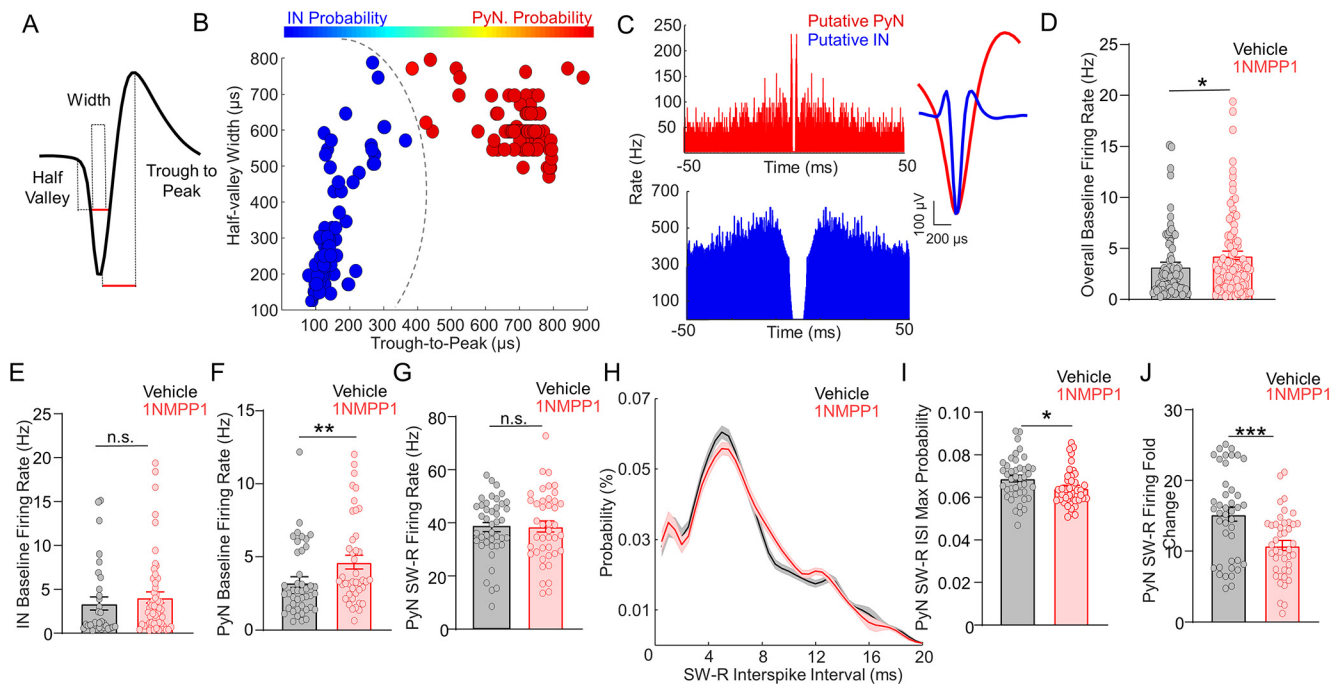


Figure 9. 1NMPP1 increases overall neuronal firing, PyN baseline, SW-R burstiness, and SW-R fold change. **A**, Schematic waveform characteristics. **B**, Pseudocolored heatmap of spike waveform characteristics [firing rate Hertz (Hz), trough-to-peak milliseconds (ms), and half-valley width (ms)] of putative PyN probability (Gaussian mixture model, $k = 2$, $n = 175$). **C**, Example of autocorrelograms of putative pyramidal (PyN) (red, top) and putative interneurons (INs) (blue, bottom), as well as waveform from putative PyN (red) and putative INs (blue). **D**, Increased overall firing rate after 1NMPP1 (red) addition compared with vehicle (black). **E**, No effect of 1NMPP1 (red) on IN overall firing compare to vehicle (black). **F**, Increased PyN firing rate after 1NMPP1 (red) compared with vehicle (black). **G**, No alteration of PyN neuron per SW-R of 1NMPP1 (red) compared to vehicle (black). **H**, Probability of PyN interspike interval (ISI) during SW-R events of vehicle (black) and 1NMPP1 (red). **I**, Decreased maximal PyN SW-R ISI probability of 1NMPP1 (red) compared with vehicle (black). **J**, Decreased PyN SW-R firing fold change of 1NMPP1 (red) compared with vehicle (black). Error bars indicate SEM. n.s., not significant. * $p < 0.05$. ** $p < 0.01$. *** $p < 0.001$.

activity (Levenga et al., 2018; Ma et al., 2019; Zhong et al., 2019; Fig. 10*Bi,Bii*). 1NMPP1, administered by two osmopumps at 0.1 $\mu\text{g/g}$ every 2 h (Fig. 10*A*), increased SW-Rs during NREM states (0.17 ± 0.02 Hz for vehicle vs 0.24 ± 0.02 Hz for 1NMPP1, $t_{(37)} = 2.17$, $p = 0.04$, unpaired t test) and wake states (0.13 ± 0.02 Hz for vehicle vs 0.25 ± 0.01 Hz for 1NMPP1, $t_{(37)} = 5.52$, $p < 0.0001$, unpaired t test; Fig. 10*C*). Interestingly, 1NMPP1-mediated increase in SW-R occurrence was greater during wake states, compared with NREM states (0.06 ± 0.02 vs 0.01 , $t_{(40)} = 2.54$, $p = 0.02$, unpaired t test; Fig. 10*D*). In agreement, the ratios of SW-R occurrence of NREM states over that of wake states were reduced by 1NMPP1, compared with vehicle (1.33 ± 0.11 for vehicle vs 0.97 ± 0.07 for 1NMPP1, $t_{(37)} = 2.74$, $p = 0.01$, unpaired t test; Fig. 10*E*). Together these data indicate that 1NMPP1 increases SW-R rates during wake states more than in NREM, suggesting that ErbB4 kinase dynamically differentially regulates SW-R occurrence at different functional states.

1NMPP1 impairs spatial working memory

To determine whether ErbB4-regulation of SW-Rs plays a role in hippocampal function, we established a W-maze (also referred to as M-maze) paradigm that tests “reference memory (inbound) and spatial working memory (outbound)” (Frank et al., 2000; Kim and Frank, 2009; Jadhav et al., 2012; Fernández-Ruiz et al., 2019). Previous studies of rats indicate that the spatial alteration task in W-maze is dependent on SW-Rs in the hippocampus (Frank et al., 2000; Kim and Frank, 2009; Jadhav et al., 2012; Fernández-Ruiz et al., 2019). We created a W-maze by 3D printing, where the two outbound arms were white and the inbound arm was black (Frank et al., 2000; Figs. 11*A*, 12*A*). T796G mice

were trained progressively to perform the W-maze behavior (Fig. 12*B*; for details, see Materials and Methods). Briefly, food-deprived mice (Fig. 11*B*) were trained to retrieve a food pellet at either end of one arm for 12 min/d until the mouse was able to retrieve food pellets without a mistake (Fig. 11*C*, usually 1–4 d). Mice were then trained to retrieve food pellets in a two-arm maze for 12 min/d from days 4 to 8 and in the W-maze beginning at day 8 until mice were able to retrieve food pellets at $>85\%$ accuracy within 12 min (Fig. 11*D,E*). One day after this criterium was achieved, T796G mice were scored for arm entries in W-maze without 1NMPP1 treatment, and on the following day, 20 min after 1NMPP1 treatment (Fig. 12*C*). As shown in Figure 12*D–G*, 1NMPP1 reduced the outbound accuracy by 18% ($91.5 \pm 0.02\%$ and $73.9 \pm 0.03\%$ without and with 1NMPP1, respectively; $t_{(6)} = 5.82$, $p = 0.001$, paired t test; Fig. 12*E*). 1NMPP1 had no effect on total outbound or inbound entries within 12 min (outbound-base 22.7 ± 1.21 , outbound-1NMPP1 21.1 ± 2.41 , inbound-base 23.1 ± 1.39 , inbound-1NMPP1 24.0 ± 3.56 , outbound $t_{(6)} = 0.72$, $p = 0.50$, inbound $t_{(6)} = 0.28$, $p = 0.79$, paired t test; Fig. 12*F,G*). Note that the inbound accuracy was not altered by 1NMPP1 ($93.2 \pm 0.03\%$ and $85.3 \pm 0.04\%$ without and with 1NMPP1, respectively; $t_{(6)} = 1.79$, $p = 0.12$, paired t test; Fig. 12*D*). 1NMPP1 had little effect on overall distance or speed (distance, 58.3 ± 7.56 and 64.1 ± 13.96 m without and with 1NMPP1, respectively; $t_{(6)} = 1.29$, $p = 0.24$, paired t test; speed, 0.08 ± 0.004 and 0.09 ± 0.01 m/s without and with 1NMPP1, respectively; $t_{(6)} = 1.38$, $p = 0.22$, paired t test; Fig. 12*H,I*). 1NMPP1 had no effect on inbound distance, time or speed (inbound distance, 25.1 ± 1.54 and 25.3 ± 2.08 m without and with 1NMPP1, respectively; $t_{(6)} = 0.12$, $p = 0.91$, paired t test; inbound time, 367.1 ± 11.82 and 345.2 ± 11.97 s without and with 1NMPP1, respectively; $t_{(6)} = 1.82$, $p = 0.12$, paired t test; inbound

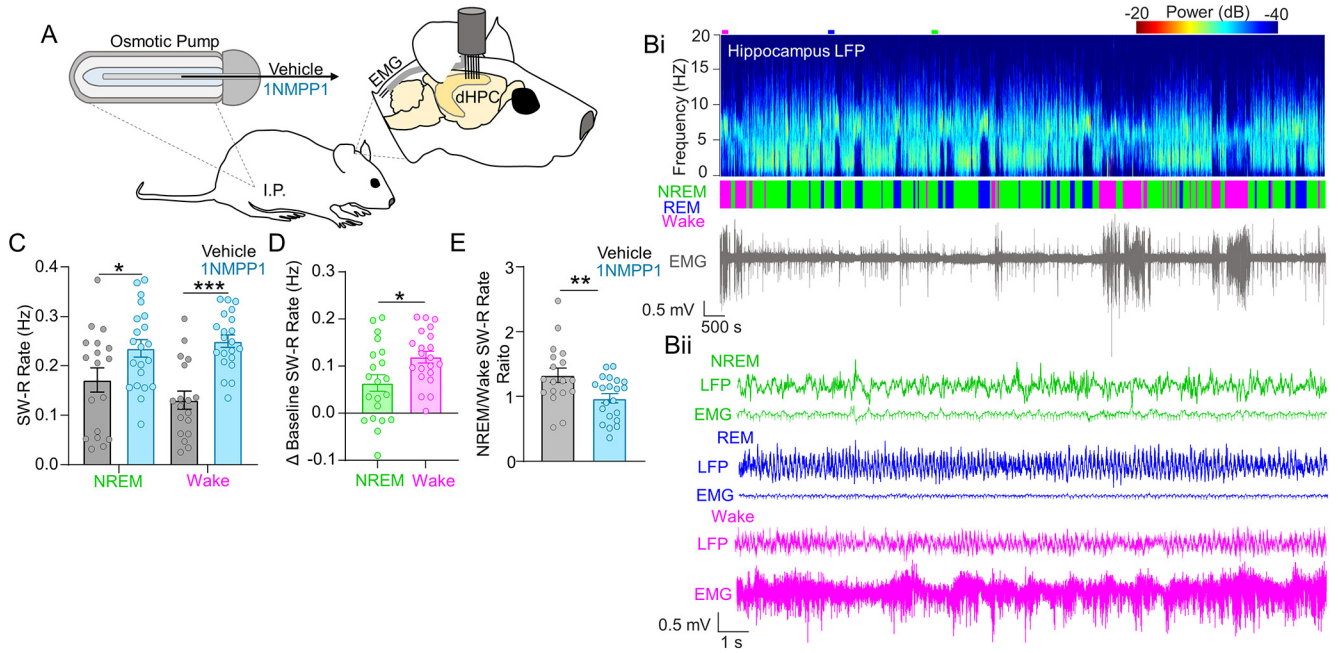


Figure 10. 1NMPP1 increases SW-R occurrence during NREM states and wake states with the largest increase during wake states. **A**, Schematic of electrode, electromyography (EMG), and osmotic pump. **Bi**, Example recordings of corresponding LFP, sleep stages, and EMG. Heatmap of power frequency (0–20 Hertz (Hz), top), classified sleep stages (non rapid eye movement (NREM) states, green; rapid eye movement (REM) states, blue; wake states, cyan, middle) and EMG (bottom). **Bii**, Example traces of local field potential (LFP) (top) and EMG (bottom) for NREM states (green, top), REM states (blue, middle), and wake states (cyan, bottom). **C**, Increased sharp wave ripple (SW-R) rate of 1NMPP1 (blue) compared with vehicle (gray) for NREM states (green, left) and wake states (cyan, right). **D**, Increased Δ baseline SW-R rate of NREM states (green) compared with wake states (cyan) of 1NMPP1 compared to vehicle. **E**, Decreased NREM-wake SW-R rate ratio of 1NMPP1 (blue) compared with vehicle (gray; vehicle: 18 recordings, 4 animals, 4–6 recordings per animal; 1NMPP1: 22 recordings, 4 animals, 4–6 recordings per animal). Error bars indicate SEM. n.s., not significant. * $p < 0.05$. ** $p < 0.01$. *** $p < 0.001$.

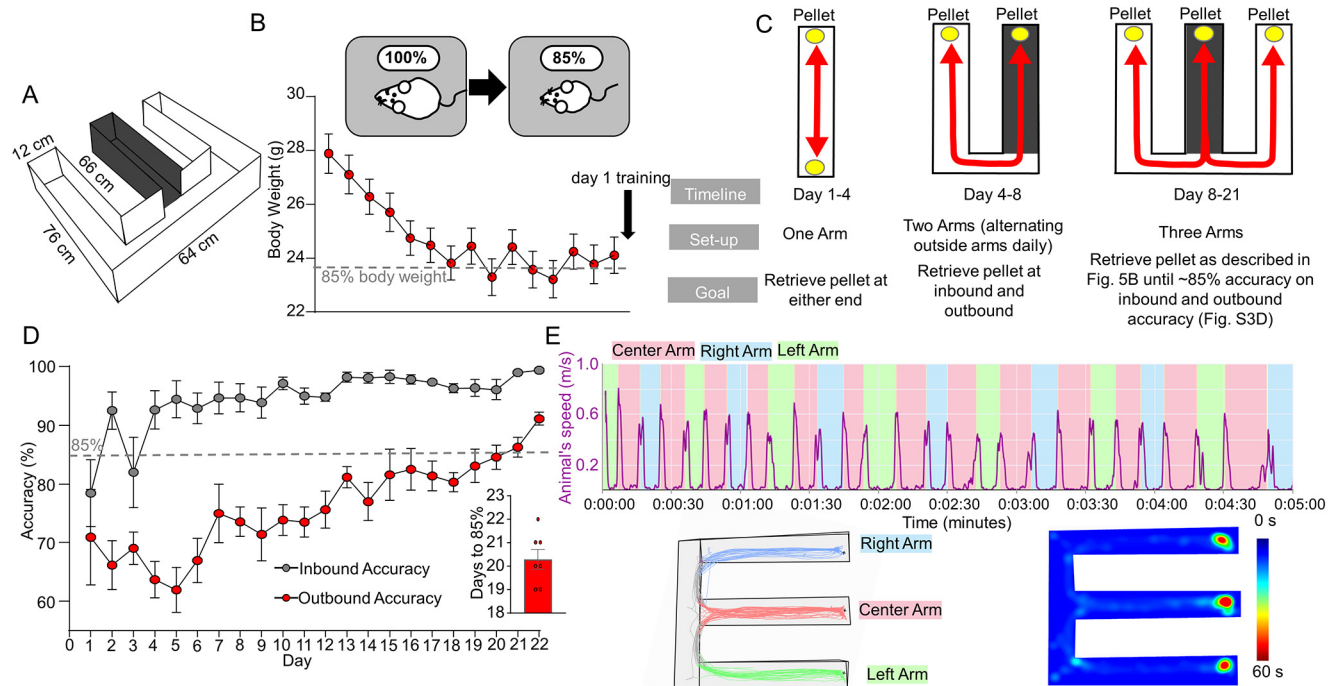


Figure 11. W-maze design, experimental paradigm and training for mice. **A**, Schematic diagrams of W-maze. **B**, Schematic diagram of mouse dieting plan. Mouse *ad libitum* body weight and after food reduction when animals body weight is 85% *ad libitum* weight (top). Body weight of animals from beginning of diet until first day of training (bottom). **C**, Schematic diagrams of W-maze training program. Days 1–4, single arm (left) retrieval of rewards at each end. Days 4–8, two-arms alternating (center) retrieval of rewards at center and outbound arm (switching outbound arm each days 4–8). Day 8 to 85% accuracy (right) retrieval of W-maze tests as described in **B**. **D**, Accuracy over three arm training of inbound (gray) and outbound (red) of animals until both inbound and outbound accuracy exceeded 85%. Inset is graphical representation of days to 85% accuracy in outbound performance (red). **E**, Graphical representation of animals' speed (purple) overlaid with arm choice (center arm, pink; right arm, blue; and left arm, green) across 5-min period of animal with >85% outbound accuracy (top). Example trace (bottom, left) in center arm, pink; right arm, blue; and left arm, green and heatmap (bottom, right) of animal with >85% outbound accuracy during 1-day behavioral test. Error bars indicate SEM.

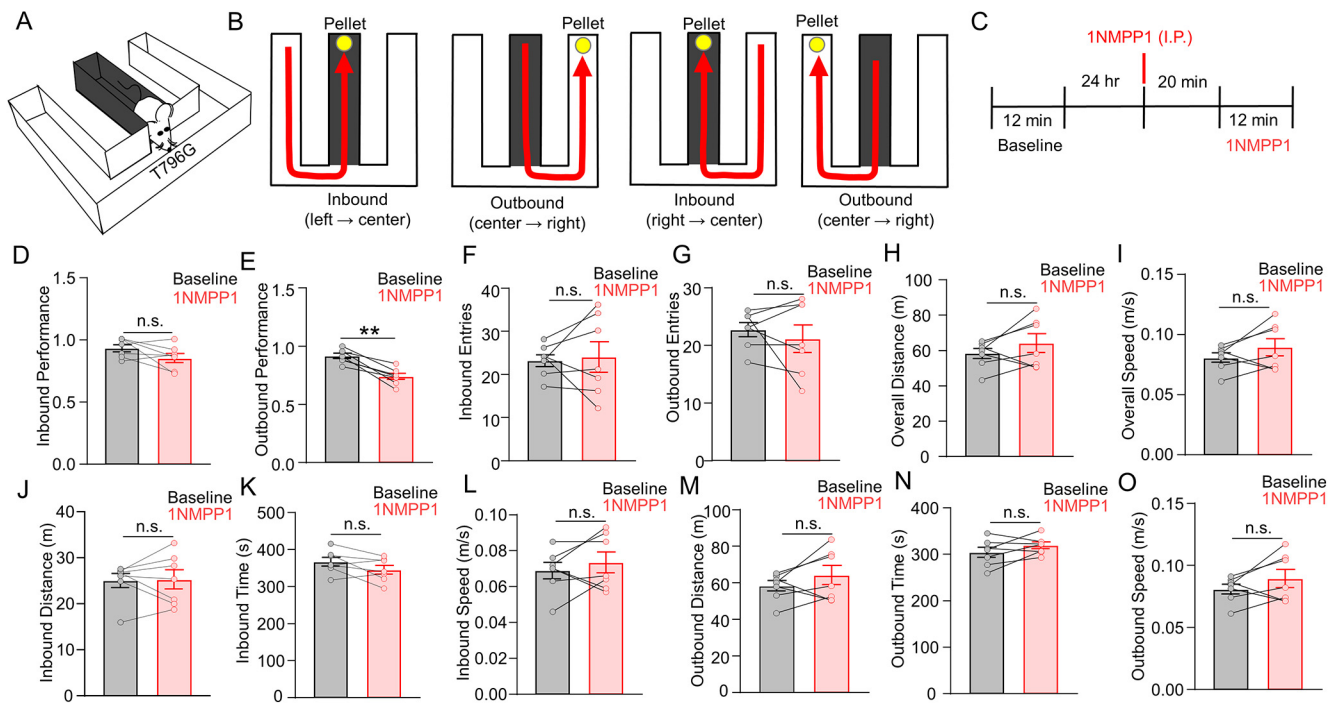


Figure 12. 1NMPP1 decreases outbound but not inbound performance in the W-maze spatial working memory tests. **A**, Schematic diagram of W-maze spatial memory task apparatus. **B**, Schematic diagrams of inbound and outbound behavior. **C**, Schematic diagram of 1NMPP1 treatment and behavioral tests. **D**, No effect of 1NMPP1 (red) on Inbound Performance compared with baseline (black). **E**, Decreased outbound performance by 1NMPP1 (red) compared with baseline (black). **F**, No effect of 1NMPP1 (red) on inbound entries compared with baseline (black). **G**, No effect of 1NMPP1 (red) on outbound entries compared with baseline (black). **H**, No effect of 1NMPP1 (red) on overall distance compared with baseline (black). **I**, No effect of 1NMPP1 (red) on overall speed compared with baseline (black). **J**, No effect of 1NMPP1 (red) on inbound distance compared with baseline (black). **K**, No effect of 1NMPP1 (red) on inbound time compared with baseline (black). **L**, No effect of 1NMPP1 (red) on inbound speed compared with baseline (black). **M**, No effect of 1NMPP1 (red) on outbound distance compared with baseline (black). **N**, No effect of 1NMPP1 (red) on outbound time compared with baseline (black). **O**, No effect of 1NMPP1 (red) on outbound speed compared with baseline [black; $n = 7$ tests baseline, 7 tests 1NMPP1 (7 mice)]. Error bars indicate SEM. n.s., not significant. ** $p < 0.01$.

speed, 0.07 ± 0.01 and 0.07 ± 0.01 m/s without and with 1NMPP1, respectively; $t_{(6)} = 0.89$ $p = 0.41$, paired t test; Fig. 12J–L). 1NMPP1 had no effect on outbound distance, time and speed (outbound distance, 25.1 ± 1.37 and 28.5 ± 2.37 m without and with 1NMPP1, respectively; $t_{(6)} = 1.46$ $p = 0.19$, paired t test; outbound time, 304.3 ± 11.00 and 319.4 ± 7.22 s without and with 1NMPP1, respectively; $t_{(6)} = 1.57$ $p = 0.17$, paired t test; outbound speed, 0.08 ± 0.004 and 0.09 ± 0.01 m/s without and with 1NMPP1, respectively; $t_{(6)} = 0.84$ $p = 0.43$, paired t test; Fig. 12M–O). These findings indicate that 1NMPP1 disrupts outbound performance in the W-maze, similar to disruption of SW-Rs (Jadhav et al., 2012) and suggest that ErbB4 kinase activity is actively needed for spatial working memory tasks.

Discussion

Our study provides evidence for a role of the NRG1-ErbB4 signaling in regulating SW-Rs. First, NRG1 decreased the occurrence of SW-Rs in hippocampal slices (Fig. 2). Second, pharmacological inhibition of ErbB4 increases the occurrence of SW-Rs *in vitro* (Fig. 3). Third, specific inhibition of chemical genetic mutant ErbB4 provides convincing evidence of increased occurrence of SW-Rs both *in vitro* and *in vivo* (Figs. 3, 6). Furthermore *in vivo*, ErbB4 also increased the firing rate of PyNs, yet decreased SW-R burstiness and SW-R firing rate fold change (Fig. 9). Interestingly, ErbB4 increased SW-Rs during both NREM states and wake states with a larger impact during wake states (Fig. 10). Importantly, acute inhibition of ErbB4 by 1NMPP1 impaired spatial working memory (Fig. 12). These findings indicate a critical role of the NRG1-ErbB4

signaling in regulating SW-Rs and reveals a novel, endogenous molecular mechanism that dynamically controls a specific network function.

SW-Rs involve a complex interaction between PyN and INs (Csicsvari et al., 1999; English et al., 2014; Stark et al., 2014; Gan et al., 2017). The activity of specific GABAergic INs in CA1 is up-regulated during SW-Rs (Klausberger et al., 2004; Royer et al., 2012; Stark et al., 2014; Varga et al., 2014). However, exactly how GABAergic transmission contributes to SW-Rs is hard to piece apart because its blockage quickly leads to an epileptic state (Maier et al., 2003; Stark et al., 2014). Nevertheless, SW-Rs are thought to be inhibited and enhanced by GABAergic agonists and antagonists, respectively. In the cortex and hippocampus, 70% of INs express ErbB4 (whereas almost all ErbB4+ cells are GABAergic INs; Woo et al., 2007; Vullhorst et al., 2009; Neddens et al., 2011; Bean et al., 2014). NGR1 promotes GABA release in the hippocampus as well as the cortex (Woo et al., 2007; Chen et al., 2010; Wen et al., 2010). ErbB4 null as well as PV+ IN-specific mutations prevent NRG1 from increasing GABA release in the hippocampus (Li et al., 2007, 2011; Wen et al., 2010). Importantly, acute perturbation of ErbB4 kinase activity reduces homeostatic GABAergic activity, suggesting that proper E-I balance requires endogenous NRG1-ErbB4 signaling in the brain. In accord, inhibition of ErbB4 rapidly reduces LTP, LFP local power and hippocampal-prefrontal cortical connectivity (Del Pino et al., 2013; Tan et al., 2018). The reduction of SW-R occurrence by ErbB4 inhibition is likely because of disrupted E-I balance in the hippocampus. ErbB4 is expressed in a variety of INs including PV+, CCK+, and VIP+ INs (Bean et al., 2014; Batista-Brito et al., 2017), ErbB4 deficiency in these cells has

been shown to decrease θ power and place field dynamics and synchrony of cortical activity (Batista-Brito et al., 2017; Del Pino et al., 2017). SW-Rs are likely regulated by ErbB4 in these INs although exact microcircuitry that NRG1-ErbB4 regulates warrants future investigation. Indeed, *in vivo* PyN firing was increased in T796G mice after 1NMPP1 treatment (Fig. 9). This is in agreement with an earlier report that acute inhibition of ErbB4 increases PyN firing by reducing GABA release (Tan et al., 2018). Intriguingly, 1NMPP1 had no detectable effect on the firing rate of INs (Fig. 9). Interpretation of this result should be careful, considering the enormously heterogeneous populations of INs and heterogeneous expression of ErbB4 in each population. It is possible that ErbB4 regulates the excitability of a subset of INs via activating Kv1.1, as shown in PFC slices (Li et al., 2011). In another study, ErbB4 inhibition reduces the excitability of dissociated ErbB4+ hippocampal INs via reducing sodium channel currents and not potassium channels (Janssen et al., 2012). Also worth noting is that NRG1 was shown to increase tritium-labeled GABA release from synaptosomes (Woo et al., 2007), suggesting that GABA release could be regulated by NRG1-ErbB4 signaling via a mechanism independent of neuronal excitability.

Our findings that ErbB4 inhibition increases the firing rate of PyNs indicate that the E-I balance in the hippocampus is critically dependent on the endogenous levels of NRG1-ErbB4 signaling. SW-Rs are associated with an increase in firing rate of PyNs (Mizuseki and Buzsáki, 2013). In accord, optogenetics activation of PyNs in the CA1 induces ripples (Stark et al., 2014). Excitatory inputs have been proposed to elicit recurrent inhibition via high-frequency oscillations (Traub et al., 1992; Ylinen et al., 1995; Taxidis et al., 2012; Malerba et al., 2016) either by feedback from local CA1 PyNs or feedforward inhibition (Schlinghoff et al., 2014; Donoso et al., 2018) driven by high excitatory drive from the CA3 (Stark et al., 2014). Such high excitatory drive is in alignment with PyN first models (Maier et al., 2011), thought to involve either chemical or axonal gap junctions (Draguhn et al., 1998; Memmesheimer, 2010). In light of increased SW-R occurrence by ErbB4 inhibition, we posit that SW-Rs are critically regulated by the NRG1-ErbB4 signaling in the hippocampus. SW-Rs mainly result from CA3 population bursts that excite CA1 PyNs via Schaffer collaterals (Ylinen et al., 1995; Csicsvari et al., 2000). ErbB4 is also expressed in the CA3 region (Bean et al., 2014) and may thus regulate the firing of CA3 PyNs by facilitating GABA release. We speculate that NRG1-ErbB4 signaling may regulate neuronal activity of PyNs in both CA3 and CA1 regions for reliable manifestation of SW-Rs.

The ability of exogenous NRG1 to increase and ErbB4 inhibition to reduce GABA release in hippocampal slices suggest that GABAergic activity is maintained at appropriate levels by the NRG1-ErbB4 signaling. Intriguingly, the maximal effects of NRG1 or ErbB4 inhibition on GABA activity are within ~30% elevation and reduction, respectively, of normal levels. Even when ErbB4 is mutated or completely inhibited, GABA activity is maintained at ~75% of normal levels in the hippocampus and PFC (Woo et al., 2007; Chen et al., 2010; Fazzari et al., 2010; Del Pino et al., 2013; Tan et al., 2018; Wang et al., 2018). Yet, ErbB4 mutation or inhibition impairs various region-specific behaviors including working memory for PFC, contextual fear conditioning for the hippocampus and tone-cued fear conditioning for the amygdala (Lu et al., 2014; Tan et al., 2018; Wang et al., 2018). These results suggest the importance of maintaining a proper level of NRG1-ErbB4 signaling.

Hippocampal activity during novelty or memory processing increases SW-R occurrence during periods of wake state immobility and NREM states of sleep (Axmacher et al., 2008; Cheng and Frank, 2008; Eschenko et al., 2008; Oliva et al., 2020). The occurrence of longer SW-Rs were found to correlate with both novelty and learning and memory (Fernández-Ruiz et al., 2019). However, molecular mechanisms that regulate SW-Rs are not well understood. SW-R occurrence increases after learning and memory tests; this change is a transient and SW-Rs return to normal levels within 60 min (Eschenko et al., 2008). These observations suggest a molecular mechanism to regulate SW-R levels. Our results indicate that the NRG1-ErbB4 signaling serves a spatial or temporal control of SW-Rs in the hippocampus. PyN activity increased during learning and memory processes (Cheng and Frank, 2008). The transcription of the NRG1 gene and release of mature NRG1 are activity dependent (Eilam et al., 1998; Liu et al., 2011; Tan et al., 2012; Mei and Nave, 2014). mRNA levels of NRG1 increase more in the CA3 region after long-term potentiation induction (Eilam et al., 1998). In particular, NRG1 Type III is expressed relatively high in the CA3 region (Fazzari et al., 2010), a region that has been implicated in originating synchronous inputs to CA1 PyNs for SW-Rs (Ylinen et al., 1995; Csicsvari et al., 2000). An increase in CA3 NRG1 would likely promote ErbB4 dependent GABA release controlling the firing of CA1 PyNs. In agreement, 1NMPP1 increases both SW-Rs (Figs. 3, 6) and CA1 PyN firing rate (Fig. 9). Additionally, 1NMPP1 impairs spatial working memory (revealed by outbound performance deficits) but had little effect on reference memory (revealed by inbound performance deficits; Fig. 12). These data allude to the need of dynamic ErbB4 kinase during spatial working memory, but not for reference memory (Wen et al., 2010; Del Pino et al., 2017).

References

- Abrahams S, Pickering A, Polkey CE, Morris RG (1997) Spatial memory deficits in patients with unilateral damage to the right hippocampal formation. *Neuropsychologia* 35:11–24.
- Axmacher N, Elger CE, Fell J (2008) Ripples in the medial temporal lobe are relevant for human memory consolidation. *Brain* 131:1806–1817.
- Batista-Brito R, Vinck M, Ferguson KA, Chang JT, Laubender D, Lur G, Mossner JM, Hernandez VG, Ramakrishnan C, Deisseroth K, Higley MJ, Cardin JA (2017) Developmental dysfunction of VIP interneurons impairs cortical circuits. *Neuron* 95:884–895.e9.
- Bean JC, Lin TW, Sathyamurthy A, Liu F, Yin D-M, Xiong W-C, Mei L (2014) Genetic labeling reveals novel cellular targets of schizophrenia susceptibility gene: distribution of GABA and non-GABA ErbB4-positive cells in adult mouse brain. *J Neurosci* 34:13549–13566.
- Bishop AC, Ubersax JA, Petsch DT, Matheos DP, Gray NS, Blethrow J, Shimizu E, Tsien JZ, Schultz PG, Rose MD, Wood JL, Morgan DO, Shokat KM (2000) A chemical switch for inhibitor-sensitive alleles of any protein kinase. *Nature* 407:395–401.
- Both M, Böhner F, O von B und H, Draguhn A (2008) Propagation of specific network patterns through the mouse hippocampus. *Hippocampus* 18:899–908.
- Broadbent NJ, Gaskin S, Squire LR, Clark RE (2010) Object recognition memory and the rodent hippocampus. *Learn Mem* 17:5–11.
- Buzsáki G (1986) Hippocampal sharp waves: their origin and significance. *Brain Res* 398:242–252.
- Buzsáki G (2015) Hippocampal sharp wave-ripple: a cognitive biomarker for episodic memory and planning. *Hippocampus* 25:1073–1188.
- Buzsáki G, Lai-Wo S L, Vanderwolf CH (1983) Cellular bases of hippocampal EEG in the behaving rat. *Brain Res Rev* 6:139–171.
- Caccavano A, Bozzelli PL, Forcelli PA, Pak DTS, Wu JY, Conant K, Vicini S (2020) Inhibitory parvalbumin basket cell activity is selectively reduced during hippocampal sharp wave ripples in a mouse model of familial Alzheimer's disease. *J Neurosci* 40:5116–5136.

- Carr MF, Karlsson MP, Frank LM (2012) Transient slow gamma synchrony underlies hippocampal memory replay. *Neuron* 75:700–713.
- Chen YJ, Zhang M, Yin DM, Wen L, Ting A, Wang P, Lu YS, Zhu XH, Li SJ, Wu CY, Wang XM, Lai C, Xiong WC, Mei L, Gao TM (2010) ErbB4 in parvalbumin-positive interneurons is critical for neuregulin 1 regulation of long-term potentiation. *Proc Natl Acad Sci USA* 107:21818–21823.
- Cheng S, Frank LM (2008) New experiences enhance coordinated neural activity in the hippocampus. *Neuron* 57:303–313.
- Csicsvari J, Hirase H, Czurkó A, Mamiya A, Buzsáki G (1999) Oscillatory coupling of hippocampal pyramidal cells and interneurons in the behaving rat. *J Neurosci* 19:274–287.
- Csicsvari J, Hirase H, Mamiya A, Buzsáki G (2000) Ensemble patterns of hippocampal CA3-CA1 neurons during sharp wave-associated population events. *Neuron* 28:585–594.
- Del Pino I, García-Frigola C, Dehorter N, Brotons-Mas JR, Alvarez-Salvado E, Martínez de Lagrán M, Ciceri G, Gabaldón MV, Moratal D, Dierssen M, Canals S, Marín O, Rico B (2013) Erbb4 deletion from fast-spiking interneurons causes schizophrenia-like phenotypes. *Neuron* 79:1152–1168.
- Del Pino I, Brotons-Mas JR, Marques-Smith A, Marighetto A, Frick A, Marín O, Rico B (2017) Abnormal wiring of CCK+ basket cells disrupts spatial information coding. *Nat Neurosci* 20:784–792.
- Diba K, Buzsáki G (2007) Forward and reverse hippocampal place-cell sequences during ripples. *Nat Neurosci* 10:1241–1242.
- Donoso JR, Schmitz D, Maier N, Kempter R (2018) Hippocampal ripple oscillations and inhibition-first network models: frequency dynamics and response to GABA modulators. *J Neurosci* 38:3124–3146.
- Draguhn A, Traub RD, Schmitz D, Jefferys JGR (1998) Electrical coupling underlies high-frequency oscillations in the hippocampus in vitro. *Nature* 394:189–192.
- Ego-Stengel V, Wilson MA (2010) Disruption of ripple-associated hippocampal activity during rest impairs spatial learning in the rat. *Hippocampus* 20:1–10.
- Eilam R, Pinkas-Kramarski R, Ratzkin BJ, Segal M, Yarden Y (1998) Activity-dependent regulation of Neu differentiation factor/neuregulin expression in rat brain. *Proc Natl Acad Sci USA* 95:1888–1893.
- English DF, Peyrache A, Stark E, Roux L, Vallentin D, Long MA, Buzsáki G (2014) Excitation and inhibition compete to control spiking during hippocampal ripples: intracellular study in behaving mice. *J Neurosci* 34:16509–16517.
- Eschenko O, Ramadan W, Mölle M, Born J, Sara SJ (2008) Sustained increase in hippocampal sharp-wave ripple activity during slow-wave sleep after learning. *Learn Mem* 15:222–228.
- Fazzari P, Paternain AV, Valiente M, Pla R, Luján R, Lloyd K, Lerma J, Marín O, Rico B (2010) Control of cortical GABA circuitry development by Nrg1 and ErbB4 signalling. *Nature* 464:1376–1380.
- Fernández-Ruiz A, Oliva A, Nagy GA, Maurer AP, Berényi A, Buzsáki G (2017) Entorhinal-CA3 dual-input control of spike timing in the hippocampus by theta-gamma coupling. *Neuron* 93:1213–1226.e5.
- Fernández-Ruiz A, Oliva A, Fermino de Oliveira E, Rocha-Almeida F, Tingley D, Buzsáki G (2019) Long-duration hippocampal sharp wave ripples improve memory. *Science* 364:1082–1086.
- Fernández-Ruiz A, Oliva A, Soula M, Rocha-Almeida F, Nagy GA, Martín-Vazquez G, Buzsáki G (2021) Gamma rhythm communication between entorhinal cortex and dentate gyrus neuronal assemblies. *Science* 372:eabf3119.
- Fisahn A, Neddens J, Yan L, Buonanno A (2009) Neuregulin-1 modulates hippocampal gamma oscillations: implications for schizophrenia. *Cereb Cortex* 19:612–618.
- Fox GE, Li M, Zhao F, Tsien JZ (2017) Distinct retrosplenial cortex cell populations and their spike dynamics during ketamine-induced unconscious state. *PLoS One* 12:e0187198.
- Frank LM, Brown EN, Wilson M (2000) Trajectory encoding in the hippocampus and entorhinal cortex. *Neuron* 27:169–178.
- Gan J, Weng S, Pernía-Andrade AJ, Csicsvari J, Jonas P (2017) Phase-locked inhibition, but not excitation, underlies hippocampal ripple oscillations in awake mice in vivo. *Neuron* 93:308–314.
- Gassmann M, Casagrande F, Orioli D, Simon H, Lai C, Klein R, Lemke G (1995) Aberrant neural and cardiac development in mice lacking the ErbB4 neuregulin receptor. *Nature* 378:390–394.
- Gillespie AK, Jones EA, Lin YH, Karlsson MP, Kay K, Yoon SY, Tong LM, Nova P, Carr JS, Frank LM, Huang Y (2016) Apolipoprotein E4 causes age-dependent disruption of slow gamma oscillations during hippocampal sharp-wave ripples. *Neuron* 90:740–751.
- Girardeau G, Benchenane K, Wiener SI, Buzsáki G, Zugaro MB (2009) Selective suppression of hippocampal ripples impairs spatial memory. *Nat Neurosci* 12:1222–1223.
- Harris KD, Henze DA, Csicsvari J, Hirase H, Buzsáki G (2000) Accuracy of tetrode spike separation as determined by simultaneous intracellular and extracellular measurements. *J Neurophysiol* 84:401–414.
- Harris KD, Hirase H, Leinekugel X, Henze DA, Buzsáki G (2001) Temporal interaction between single spikes and complex spike bursts in hippocampal pyramidal cells. *Neuron* 32:141–149.
- Huang YZ, Won S, Ali DW, Wang Q, Tanowitz M, Du QS, Pelkey KA, Yang DJ, Xiong WC, Salter MW, Mei L (2000) Regulation of neuregulin signaling by PSD-95 interacting with ErbB4 at CNS synapses. *Neuron* 26:443–455.
- Jadhav SP, Kemere C, German PW, Frank LM (2012) Awake hippocampal sharp-wave ripples support spatial memory. *Science* 336:1454–1458.
- Janssen MJ, Leiva-Salcedo E, Buonanno A (2012) Neuregulin directly decreases voltage-gated sodium current in hippocampal ErbB4-expressing interneurons. *J Neurosci* 32:13889–13895.
- Joo HR, Frank LM (2018) The hippocampal sharp wave-ripple in memory retrieval for immediate use and consolidation. *Nat Rev Neurosci* 19:744–757.
- Karlsson MP, Frank LM (2008) Network dynamics underlying the formation of sparse, informative representations in the hippocampus. *J Neurosci* 28:14271–14281.
- Karlsson MP, Frank LM (2009) Awake replay of remote experiences in the hippocampus. *Nat Neurosci* 12:913–918.
- Kay K, Frank LM (2019) Three brain states in the hippocampus and cortex. *Hippocampus* 29:184–238.
- Kay K, Sosa M, Chung JE, Karlsson MP, Larkin MC, Frank LM (2016) A hippocampal network for spatial coding during immobility and sleep. *Nature* 531:185–190.
- Kim SM, Frank LM (2009) Hippocampal lesions impair rapid learning of a continuous spatial alternation task. *PLoS One* 4:e5494.
- Klausberger T, Somogyi P (2008) Neuronal diversity and temporal dynamics: the unity of hippocampal circuit operations. *Science* 321:53–57.
- Klausberger T, Márton LF, Baude A, Roberts JDB, Magill PJ, Somogyi P (2004) Spike timing of dendrite-targeting bistratified cells during hippocampal network oscillations in vivo. *Nat Neurosci* 7:41–47.
- Koprivica V, Cho K-S, Park JB, Yiu G, Atwal J, Gore B, Kim JA, Lin E, Tessier-Lavigne M, Chen DF, He Z (2005) EGFR activation mediates inhibition of axon regeneration by myelin and chondroitin sulfate proteoglycans. *Science* 310:106–110.
- Levenga J, Peterson DJ, Cain P, Hoeffler CA (2018) Sleep behavior and EEG oscillations in aged Dp(16)1Yey/+ mice: a down syndrome model. *Neuroscience* 376:117–126.
- Li KX, Lu YM, Xu ZH, Zhang J, Zhu JM, Zhang JM, Cao SX, Chen XJ, Chen Z, Luo JH, Duan S, Li XM (2011) Neuregulin 1 regulates excitability of fast-spiking neurons through Kv1.1 and acts in epilepsy. *Nat Neurosci* 15:267–273.
- Li B, Woo RS, Mei L, Malinow R (2007) The neuregulin-1 receptor ErbB4 controls glutamatergic synapse maturation and plasticity. *Neuron* 54:583–597.
- Lin L, Chen G, Xie K, Zaia KA, Zhang S, Tsien JZ (2006) Large-scale neural ensemble recording in the brains of freely behaving mice. *J Neurosci Methods* 155:28–38.
- Liu X, Bates R, Yin DM, Shen C, Wang F, Su N, Kirov SA, Luo Y, Wang JZ, Xiong WC, Mei L (2011) Specific regulation of NRG1 isoform expression by neuronal activity. *J Neurosci* 31:8491–8501.
- Lu Y, Sun XD, Hou FQ, Bi LL, Yin DM, Liu F, Chen YJ, Bean JC, Jiao HF, Liu X, Li BM, Xiong WC, Gao TM, Mei L (2014) Maintenance of GABAergic activity by neuregulin 1-ErbB4 in amygdala for fear memory. *Neuron* 84:835–846.
- Ma C, Zhong P, Liu D, Barger ZK, Zhou L, Chang WC, Kim B, Dan Y (2019) Sleep regulation by neurotensinergic neurons in a thalamo-amygdala circuit. *Neuron* 103:323–334.e7.
- Maguire EA, Burgess N, Donnett JG, Frackowiak RS, Frith CD, O'Keefe J (1998) Knowing where and getting there: a human navigation network. *Science* 280:921–924.

- Maier N, Nimrich V, Draguhn A (2003) Cellular and network mechanisms underlying spontaneous sharp wave-ripple complexes in mouse hippocampal slices. *J Physiol* 550:873–887.
- Maier N, Morris G, Johanning FW, Schmitz D (2009) An approach for reliably investigating hippocampal sharp wave-ripples in vitro. *PLoS One* 4:e6925.
- Maier N, Tejero-Cantero Á, Dorn AL, Winterer J, Beed PS, Morris G, Kempter R, Poulet JFA, Leibold C, Schmitz D (2011) Coherent phasic excitation during hippocampal ripples. *Neuron* 72:137–152.
- Malerba P, Krishnan GP, Fellous JM, Bazhenov M (2016) Hippocampal CA1 ripples as inhibitory transients. *PLoS Comput Biol* 12:e1004880.
- Mei L, Nave KA (2014) Neuregulin-ERBB signaling in the nervous system and neuropsychiatric diseases. *Neuron* 83:27–49.
- Mei L, Xiong WC (2008) Neuregulin 1 in neural development, synaptic plasticity and schizophrenia. *Nat Rev Neurosci* 9:437–452.
- Memmesheimer R-M (2010) Quantitative prediction of intermittent high-frequency oscillations in neural networks with supralinear dendritic interactions. *Proc Natl Acad Sci USA* 107:11092–11097.
- Mizuseki K, Buzsáki G (2013) Preconfigured, skewed distribution of firing rates in the hippocampus and entorhinal cortex. *Cell Rep* 4:1010–1021.
- Mizuseki K, Sirota A, Pastalkova E, Buzsáki G (2009) Theta oscillations provide temporal windows for local circuit computation in the entorhinal-hippocampal loop. *Neuron* 64:267–280.
- Mizuseki K, Diba K, Pastalkova E, Buzsáki G (2011) Hippocampal CA1 pyramidal cells form functionally distinct sublayers. *Nat Neurosci* 14:1174–1181.
- Neddens J, Fish KN, Tricoire L, Vullhorst D, Shamir A, Chung W, Lewis DA, McBain CJ, Buonanno A (2011) Conserved interneuron-specific ErbB4 expression in frontal cortex of rodents, monkeys, and humans: implications for schizophrenia. *Biol Psychiatry* 70:636–645.
- Nitzan N, McKenzie S, Beed P, English DF, Oldani S, Tukker JJ, Buzsáki G, Schmitz D (2020) Propagation of hippocampal ripples to the neocortex by way of a subiculum-retrosplenial pathway. *Nat Commun* 11:1947.
- Norimoto H, Mizunuma M, Ishikawa D, Matsuki N, Ikegaya Y (2012) Muscarinic receptor activation disrupts hippocampal sharp wave-ripples. *Brain Res* 1461:1–9.
- Norimoto H, Matsumoto N, Miyawaki T, Matsuki N, Ikegaya Y (2013) Subicular activation preceding hippocampal ripples in vitro. *Sci Rep* 3:2696.
- Norimoto H, Makino K, Gao M, Shikano Y, Okamoto K, Ishikawa T, Sasaki T, Hioki H, Fujisawa S, Ikegaya Y (2018) Hippocampal ripples down-regulate synapses. *Science* 359:1524–1527.
- O'Neill J, Senior T, Csicsvari J (2006) Place-selective firing of CA1 pyramidal cells during sharp wave/ripple network patterns in exploratory behavior. *Neuron* 49:143–155.
- Oliva A, Fernández-Ruiz A, Oliveira EF, de Buzsáki G (2018) Origin of gamma frequency power during hippocampal sharp-wave ripples. *Cell Rep* 25:1693–1700.e4.
- Oliva A, Fernández-Ruiz A, Leroy F, Siegelbaum SA (2020) Hippocampal CA2 sharp-wave ripples reactivate and promote social memory. *Nature* 587:264–266.
- Ozaki M, Itoh K, Miyakawa Y, Kishida H, Hashikawa T (2004) Protein processing and releases of neuregulin-1 are regulated in an activity-dependent manner. *J Neurochem* 91:176–188.
- Papatheodoropoulos C, Sotiriou E, Kotzadimitriou D, Drimala P (2007) At clinically relevant concentrations the anaesthetic/amnesic thiopental but not the anticonvulsant phenobarbital interferes with hippocampal sharp wave-ripple complexes. *BMC Neurosci* 8:60.
- Pitcher GM, Beggs S, Woo R-S, Mei L, Salter MW (2008) ErbB4 is a suppressor of long-term potentiation in the adult hippocampus. *Neuroreport* 19:139–143.
- Redish AD, Schmitzer-Torbert NC (2002) MCLUSTspike sorting toolbox, version 3.0. Available at <http://www.cbc.umn.edu/redish/mclust/>.
- Rothschild G, Eban E, Frank LM (2017) A cortical-hippocampal-cortical loop of information processing during memory consolidation. *Nat Neurosci* 20:251–259.
- Royer S, Zemelman BV, Losonczy A, Kim J, Chance F, Magee JC, Buzsáki G (2012) Control of timing, rate and bursts of hippocampal place cells by dendritic and somatic inhibition. *Nat Neurosci* 15:769–775.
- Schlingloff D, Káli S, Freund TF, Hájos N, Gulyás AI (2014) Mechanisms of sharp wave initiation and ripple generation. *J Neurosci* 34:11385–11398.
- Schmitzer-Torbert N, Redish AD (2004) Neuronal activity in the rodent dorsal striatum in sequential navigation: separation of spatial and reward responses on the multiple T task. *J Neurophysiol* 91:2259–2272.
- Schmitzer-Torbert N, Jackson J, Henze D, Harris K, Redish AD (2005) Quantitative measures of cluster quality for use in extracellular recordings. *Neuroscience* 131:1–11.
- Spellman T, Rigotti M, Ahmari SE, Fusi S, Gogos JA, Gordon JA (2015) Hippocampal-prefrontal input supports spatial encoding in working memory. *Nature* 522:309–314.
- Stark E, Eichler R, Roux L, Fujisawa S, Rotstein HG, Buzsáki G (2013) Inhibition-induced theta resonance in cortical circuits. *Neuron* 80:1263–1276.
- Stark E, Roux L, Eichler R, Senzai Y, Royer S, Buzsáki G (2014) Pyramidal cell-interneuron interactions underlie hippocampal ripple oscillations. *Neuron* 83:467–480.
- Tan GH, Liu YY, Hu XL, Yin DM, Mei L, Xiong ZQ (2012) Neuregulin 1 represses limbic epileptogenesis through ErbB4 in parvalbumin-expressing interneurons. *Nat Neurosci* 15:258–266.
- Tan Z, Robinson HL, Yin DM, Liu Y, Liu F, Wang H, Lin TW, Xing G, Gan L, Xiong WC, Mei L (2018) Dynamic ErbB4 activity in hippocampal-prefrontal synchrony and top-down attention in rodents. *Neuron* 98:380–393.e4.
- Taxidis J, Coombes S, Mason R, Owen MR (2012) Modeling sharp wave-ripple complexes through a CA3-CA1 network model with chemical synapses. *Hippocampus* 22:995–1017.
- Traub RD, Miles R, Buzsáki G (1992) Computer simulation of carbachol-driven rhythmic population oscillations in the CA3 region of the in vitro rat hippocampus. *J Physiol* 451:653–672.
- Varga C, Ojiala M, Lish J, Szabo GG, Bezaire M, Marchionni I, Golshani P, Soltesz I (2014) Functional fission of parvalbumin interneuron classes during fast network events. *Elife* 3:e04006.
- Vullhorst D, Neddens J, Karavanova I, Tricoire L, Petralia RS, McBain CJ, Buonanno A (2009) Selective expression of ErbB4 in interneurons, but not pyramidal cells, of the rodent hippocampus. *J Neurosci* 29:12255–12264.
- Wang H, Liu F, Chen W, Sun X, Cui W, Dong Z, Zhao K, Zhang H, Li H, Xing G, Fei E, Pan BX, Li BM, Xiong WC, Mei L (2018) Genetic recovery of ErbB4 in adulthood partially restores brain functions in null mice. *Proc National Acad Sci* 115:201811287.
- Wen L, Lu YS, Zhu XH, Li XM, Woo RS, Chen YJ, Yin DM, Lai C, Terry AV, Vazdarjanova A, Xiong WC, Mei L (2010) Neuregulin 1 regulates pyramidal neuron activity via ErbB4 in parvalbumin-positive interneurons. *Proc Natl Acad Sci USA* 107:1211–1216.
- Whishaw IQ, Vanderwolf CH (1971) Hippocampal EEG and behavior: effects of variation in body temperature and relation of EEG to vibrissae movement, swimming and shivering. *Physiol Behav* 6:391–397.
- Wilson M, McNaughton B (1994) Reactivation of hippocampal ensemble memories during sleep. *Science* 265:676–679.
- Woo RS, Li XM, Tao Y, Carpenter-Hyland E, Huang YZ, Weber J, Neiswender H, Dong XP, Wu J, Gassmann M, Lai C, Xiong WC, Gao TM, Mei L (2007) Neuregulin-1 enhances depolarization-induced GABA release. *Neuron* 54:599–610.
- Ylinen A, Bragin A, Nádasdy Z, Jandó G, Szabó I, Sik A, Buzsáki G (1995) Sharp wave-associated high-frequency oscillation (200 Hz) in the intact hippocampus: network and intracellular mechanisms. *J Neurosci* 15:30–46.
- Zhong P, Zhang Z, Barger Z, Ma C, Liu D, Ding X, Dan Y (2019) Control of non-REM sleep by midbrain neurotensinergic neurons. *Neuron* 104:795–809.e6.